UNIVERSITA' VITA-SALUTE SAN RAFFAELE

CORSO DI DOTTORATO DI RICERCA INTERNAZIONALE IN MEDICINA MOLECOLARE

CURRICULUM IN MEDICINA CLINICA E SPERIMENTALE

ENDOSCOPIC ULTRASOUND BEYOND MORPHOLOGY: FEASIBILITY OF TRANSCRIPTOMIC ANALYSIS AND THE ROLE OF DEEP LEARNING MODELS AND MICROVASCULARIZATION STUDY IN THE DIAGNOSIS AND PROGNOSIS OF PANCREATIC NEUROENDOCRINE NEOPLASMS

DoS: Prof. Paolo Giorgio Arcidiacono

Second Supervisor: Prof. Andrea Laghi

Tesi di DOTTORATO di RICERCA di Matteo Tacelli

matr. 017374

Ciclo di dottorato XXXVI

SSD MED/12

Anno Accademico 2022/2023

CONSULTAZIONE TESI DI DOTTORATO DI RICERCA

Il sottoscritto MATTEO TACELLI

Matricola / *registration number* 017374

nato a/ *born at* SAN PIETRO VERNOTICO (BR)

il/*on* *12/05/1989*

autore della tesi di Dottorato di ricerca dal titolo / *author of the PhD Thesis titled*

"Endoscopic Ultrasound Beyond Morphology: Feasibility of Transcriptomic Analysis and the Role of Deep Learning Models and Microvascularization Study in the Diagnosis and Prognosis of Pancreatic Neuroendocrine Neoplasms"

AUTORIZZA la Consultazione della tesi / AUTHORIZES *the public release of the thesis*

Data /Date 09/11/2023

Firma /Signature

DECLARATION

This thesis has been:

- composed by myself and has not been used in any previous application for a degree. Throughout the text I use both 'I' and 'We' interchangeably.

- has been written according to the editing guidelines approved by the University.

Permission to use images and other material covered by copyright has been sought and obtained. For the following image/s (specify), it was not possible to obtain permission and is/are therefore included in thesis under the "fair use" exception (Italian legislative Decree no. 68/2003). All the results presented here were obtained by myself, except for:

1) ***Quantification of RNA concentration and RIN.*** *Obtained in collaboration with Dr. Tresoldi Cristina, Center of Biological Resources, San Raffaele Hospital. In this project I personally performed all the endoscopic procedures and biopsies, collected patient data, performed RNA extraction of all samples included in Method 1 and performed statistical analysis.*

2) ***Elaboration of the algorithm for artificial intelligence analysis.*** *Obtained in collaboration with CAMMA (Computational Analysis and Modeling of Medical Activities, Responsible Dr N. Padoy) from the Institut de Chirurgie Guidée par l'Image (IHU) in Strasbourg, France*

3) ***Assessment of Microvessel Density.*** *Obtained in collaboration with Surgery Unit of San Raffaele Hospital (Director Prof. M. Falconi). In this project I personally performed the endoscopic procedures of the included patients, retrospectively re-evaluated all contrast uptake videos, compared these videos with the IHC expression of MVD.* Some of these data were already published in the paper: Preoperative assessment of microvessel density in nonfunctioning pancreatic neuroendocrine tumors (NF-PanNETs), Battistella A et al, Surgery. 2022;172(4):1236-1244

All sources of information are acknowledged by means of reference.

ABSTRACT

This dissertation delves into the application of advanced diagnostic techniques in the evaluation of pancreatic neuroendocrine neoplasms (PanNENs), overcoming traditional Endoscopic Ultrasound (EUS) approaches. PanNENs range prognostically from an indolent pattern to aggressive and metastasizing grade of malignancies, with progression determined by tumor grading and staging. The grading system is based on the mitotic index and the Ki-67 index.

EUS stands out in the diagnosis and management of PanNENs, offering biopsy options for cytologic (EUS-FNA) or histologic (EUS-FNB) evaluations. Its specificity is enhanced through ancillary techniques like elastography and contrast-enhanced EUS (CE-EUS). Despite EUS-FNA represent the gold standard for grading, there is still a considerable grading misclassification in PanNENs and so it is necessary to find innovations in EUS application. So, this thesis targets three objectives in this sense: (1) to assess the possibility to obtain RNA in good quantity and quality from PanNENs EUS-FNA samples; (2) to provide a quantitative assessment of contrast uptake and predict microvessel density (MVD) via EUS-CE; and (3) to employ deep learning models for EUS differential diagnosis of pancreatic solid neoplasms.

RNA extraction from EUS-FNA is explored by comparing three RNA preservation and extraction methods. The global median RNA concentration was 11,000 pg/μL, with the highest yields obtained using the Snap Frozen + Trizol method. RNA Integrity Number (RIN) values also varied significantly across methods, with Snap frozen + 1-Thioglycerol method being the most accurate.

The microvascularization sub-project included patients undergoing EUS-CE at San Raffaele Hospital for PanNENs or PDACs. We used VueBox® software to analyze post-procedure DICOM videos, yielding parameters related to contrast medium uptake. A cohort of 73 patients with focal pancreatic was considered and we found notable differences between PDAC and PanNENs in the most of variables associated with contrast uptake. Furthermore, we considered a retrospective cohort study of NF-PanNEN patients undergone surgical resection and we correlated EUS-CE enhancement patterns

with MVD, showing that the low MVD was associated with an arterial hypoenhancement pattern at EUS-CE and a higher Ki67 index.

For the differential diagnosis of pancreatic neoplasms, deep learning algorithms analyzed images segmentated by expert endosonographers. Two models were developed, with Model 1 showing an average precision of 87.5% for classification, while Model 2 demonstrated 88.9% precision with improved specificity.

In conclusion, this thesis advances the understanding of PanNENs by integrating transcriptomic analysis, microvascularization assessment, and AI into diagnostic and prognostic processes. The findings highlight the potential for precision medicine in gastroenterology and the need for future research to develop AI models that synthesize comprehensive patient data, ensuring a holistic approach to patient care and enhancing the diagnostic and therapeutic outlook for PanNENs.

TABLE OF CONTENTS

ACRONYMS AND ABBREVIATIONS

PanNEN: pancreatic neuroendocrine tumor

VIP: vasoactive intestinal peptide

NF-PanNEN: nonfunctional pancreatic neuroendocrine tumor

ENETS: European Neuroendocrine Tumor Society

VHL: von Hippel-Lindau

MEN-1: multiple endocrine neoplasia type I

WHO: World Health Organization

AJCC: American Joint Committee on Cancer

G: grading

TNM: Tumour Node Metastasis

EUS: Endoscopic Ultrasound

FNA: fine needle aspiration

FNB: Fine needle biopsy

ROSE: Rapid-On-Site Evaluation

CT-scan: Computed Tomography scan

MRI: Magnetic resonance imaging

CE-EUS: Contrast enhanced endoscopic ultrasound

EUS-E: endoscopic ultrasound elastography

AI: artificial intelligence

MVD: microvascular density

RNA: RiboNucleic Acid

DNA: DeoxyriboNucleic Acid

RT-qPCR: real-time quantitative polymerase chain reaction

RNA-Seq: RNA Sequencing

PDAC: Pancreatic Ductal Adenocarcinoma

EUS-TA: EUS-guided tissue acquisition

RIN: RNA integrity number

BMI: Body Mass Index

PE: Peak enhancement

WiAUC: Area under the curve during Wash-in

RT: Rise time

mTT: Mean transit time

TTP: Time to peak

WiR: Wash-in rate

WiPI: Wash-in perfusion index

WoAUC: Area under the curve during Wash-out

WiWoAUC: Wash-in and Wash-out AUC – AUC Wash-in e Wash-out

ML: machine learning

ANNs: artificial neural networks

ES: expert systems

DL: deep learning

LIST OF FIGURES AND TABLES

INTRODUCTION

Basic anatomy of the pancreas

The pancreas is a median parenchymatous organ located horizontally on the posterior wall of the abdomen, retroperitoneally, extending from the duodenal C loop to the hilum of the spleen. Its right end (called the "head") is separated from the "body" by the pancreatic incisura. The "tail" is the extreme left, thinned part.

The head is strictly adherent to the duodenal C, which contours it. In the posterior face of the head of the pancreas is located the common bile duct. Through the fibrous lamina of Treitz, the head of the pancreas has a relationship with the right crus of the diaphragm, the inferior vena cava, the terminal part of the right renal vein and the aorta. The sub-mesocolic portion of the head of the pancreas extends downward to the uncinate process, which is surmounted by the superior mesenteric vessels.

The body of the pancreas corresponds posteriorly to the first two lumbar vertebrae. It is in contact, posteriorly, with the medial and intermediate pillars of the diaphragm and with the superior mesenteric artery, which originates at this level from the aorta.

The body of the pancreas is also in contact with the splenic vein and the superior mesenteric vein.

The anterior surface of the body of the pancreas is covered by the peritoneum, which forms the posterior wall of the omental bursa and is in relation to the posterior surface of the body of the stomach.

The upper edge is in relation to the celiac trunk and the splenic artery. The tail of the pancreas lies in the pancreatic-splenic ligament together with the splenic vessels.

The pancreas is an amphipathic gland with an exocrine component consisting of the pancreatic acini and an endocrine component consisting of the pancreatic islets of Langerhans. The exocrine component is responsible for processing the pancreatic juice, which is released through the branch pancreatic duct system into the main ducts, namely Wirsung and Santorini. The Wirsung duct flows into the papilla major of the duodenum, while the accessory Santorini duct originates from the main duct at the level of the pancreatic neck and flows into the papilla minor of the duodenum. The endocrine component of the pancreas consists of pancreatic islets, which are mostly located into the tail ([Anatomia umana] / Giuseppe C. Balboni ...[et al.] - Università degli Studi di Firenze).

Pancreatic Neuroendocrine Neoplasms

Pancreatic neuroendocrine tumors (PanNENs) consist of a diverse array of tumors originating from the endocrine cells within the pancreas. Initially identified as islet cell tumors based on their assumed origin in the pancreatic islets of Langerhans, they represent a minority of pancreatic cancer cases, accounting for less than 2% of these cancers and about 7% of all neuroendocrine tumors throughout the body (Lawrence *et al*, 2011). While these tumors are rare, with an occurrence of at most 1 case per 100,000 people annually, there has been a notable rise in their diagnosis recently (Bilimoria *et al*, 2007; Goh *et al*, 2011). This uptick is likely due to the more frequent use of advanced imaging techniques and the higher discovery rate of unexpected pancreatic masses, known as pancreatic incidentalomas (Hallet *et al*, 2015; Kimura *et al*, 1991; Yao *et al*, 2008; Partelli *et al*, 2019). PanNENs can develop at any stage in life but are most commonly identified in individuals between 40 and 65 years old. There is some controversy regarding the cell of origin of PanNENs. PanNENs are often referred to as "islet tumors," although it is not certain that they originate from pancreatic islets. These tumors often contain tubular structures and often produce one or more hormones not normally found in the adult pancreas, such as gastrin and vasoactive intestinal peptide (VIP). The finding of ductal structures in many PanNENs and the budding of endocrine cells from ducts during pancreatic ontogeny have led to the hypothesis that these tumors are ductal in origin. More recently, it has been hypothesized that these tumors arise from stem cells capable of neuroendocrine differentiation. Cancer stem cells are important in the pathogenesis of several solid tumors, and a recent study reports their presence in GI NETs (Cives & Strosberg, 2018).

These tumors are categorized based on whether they produce hormones, with functional PanNENs (F-PanNENs) releasing hormones like insulin, gastrin, glucagon, and vasoactive intestinal peptide (VIP) that lead to various clinical conditions. On the other hand, nonfunctional PanNENs (NF-PanNENs) do not lead to such syndromes, even though they may still secrete multiple peptides. Notably, NF-PanNENs represent the bulk of PanNENs, comprising 50–75% of cases (Jensen *et al*, 2008; Metz & Jensen, 2008).

While most PanNENs occur sporadically, about 10% are linked to inherited genetic disorders. These tumors are highly prevalent in patients with multiple endocrine neoplasia

type I (MEN-1), where NF-PanNENs, gastrinomas, and insulinomas are particularly common, occurring in 80-100% of these patients. Additionally, NF-PanNENs are seen in around 20% of individuals with von Hippel-Lindau (VHL) syndrome. Patients with neurofibromatosis type I and tuberous sclerosis may also develop PanNENs, though less frequently. Tumors arising within hereditary syndromes typically progress more slowly than those that occur randomly (Jensen *et al*, 2008).

NF-PanNENs exhibit a broad spectrum of clinical activity. They can present as non-invasive, gradually expanding growths, aggressively spreading local invasions, or rapidly metastasizing malignancies. The biological progression of both F-PanNENs and NF-PanNENs is determined by their respective grades and stages. The initial WHO criteria for classifying pancreatic neuroendocrine tumors (PanNENs) were established in 2000. In 2010, the classification was updated to integrate the term 'neuroendocrine' and to incorporate the grading system developed by the European Neuroendocrine Tumor Society (ENETS), which focuses on tumor proliferation. This system categorizes tumors into three levels based on the rate of cell division as measured by mitotic counts and the Ki-67 proliferation index. The effectiveness of this grading system in predicting outcomes has been confirmed by multiple extensive research studies (Perri *et al*, 2019). A newer WHO classification was adopted in 2017, which adjusts the Ki-67 index threshold for G2 tumors to 3% and further distinguishes between two groups of G3 tumors based on their histopathological differentiation (Klöppel *et al*, 2017; Klimstra *et al*, 2010).

Staging of PanNENs, like that of other cancers, is conducted using the TNM system, which assesses tumor size, lymph node involvement, and metastasis. While the WHO classification predicts the biological behavior of the tumors, the TNM system forecasts patient outcomes based on the anatomical spread of the disease. Previous TNM staging included versions from the 7th edition of the American Joint Committee on Cancer (AJCC) staging manual and another by ENETS. As of 2019, the 8th edition of the AJCC staging manual is the standard for anatomical staging (Rindi *et al*, 2012a; Falconi *et al*, 2016; Sorbye *et al*, 2014).

A recent comprehensive population-based study has highlighted that both tumor grade and stage are essential for determining the prognosis of patients with PanNENs. Survival rates over five years can vary widely from 55% for those with localized, surgically removed PanNENs to 15% for those with inoperable tumors. Median overall survival

times also differ significantly, ranging from approximately 12 years for patients with Grade 1 PanNENs down to 10 months for those with Grade 3 tumors (Dasari *et al*, 2017; Perri *et al*, 2019).

Basics of endoscopic ultrasound in pancreatic neoplasms

Endoscopic Ultrasound (EUS) is a technique that combines the use of an endoscopic instrument with ultrasound. With this technique it is possible to study the anatomical structures around the upper gastrointestinal tract, from the esophagus to the duodenum (pancreas, biliary tract, gallbladder, walls of the gastrointestinal tract, left liver lobe, splenic hilum, aorta, kidney and left adrenal gland), as well as the perirectal structures.

One of the main indications for EUS is the study of the pancreatic parenchyma and ducts. In fact, the pancreas, due to its deep retroperitoneal location, has always been a difficult organ to access and study, especially with transcutaneous ultrasound techniques (US)(Dimagno *et al*, 1980; Harewood & Wiersema, 2002).

EUS is undoubtedly the most sensitive imaging technique in the diagnosis of solid and cystic pancreatic neoplasms. This has been demonstrated by various articles over the years, despite the relatively short history of the technique (Canto *et al*, 2004, 2012; Loos *et al*, 2012; Harinck *et al*, 2016; Yamada *et al*, 2023). A recent literature review attempted to collect all articles that evaluated the differences in sensitivity between EUS and other techniques(Kitano *et al*, 2019). In this paper, 22 different articles were reported, and the pooled sensitivity of EUS in obtaining a diagnosis of pancreatic neoplasm was 94%, compared with the sensitivity of CT-scan (74%), US (67%), and Magnetic Resonance Imaging (MRI; 79%). This finding is even more relevant for small lesions, where contrast-enhanced CT-scan fails to detect between 47% and 60% of tumors (Müller *et al*, 1994; Ainsworth *et al*, 2003; Borbath *et al*, 2005; Kamata *et al*, 2014; DeWitt *et al*, 2004; Agarwal *et al*, 2004). A 2017 meta-analysis (Krishna *et al*, 2017) then pooled studies evaluating the diagnostic ability of EUS in malignant pancreatic lesions when CT-scan findings were indeterminate, showing sensitivity, specificity, and diagnostic accuracy of 85%, 58%, and 75%, respectively. Therefore, international guidelines recommend the use of EUS in the diagnosis of solid pancreatic neoplasms (with higher or lower levels of evidence) (Ducreux *et al*, 2015; Dumonceau *et al*, 2017; Okusaka *et al*, 2020).

In addition to its diagnostic superiority over other imaging modalities, EUS is included in the management algorithm of patients with solid pancreatic lesions because of the possibility of biopsy sampling for cytologic (EUS-fine needle aspiration; FNA) or histologic (EUS-fine needle biopsy; FNB) evaluation of lesions. This is a not negligeable advantage, as it allows a complete diagnostic evaluation to be performed in a single session, thus gaining useful time to start curative treatments earlier. Four different meta-analyses evaluated the sensitivity and specificity of EUS-FNA in the diagnosis of solid pancreatic lesions, which were 85-92% and 96-98%, respectively (Hewitt *et al*, 2012; Chen *et al*, 2012; Puli *et al*, 2013; Banafea *et al*, 2016). In contrast, in small-diameter neoplasms, the studies available to date are few and often contradictory, but in general there is a trend toward a physiologic decrease in sensitivity with a fairly stable specificity (40-100% and 80-100%, respectively) (Uehara *et al*, 2011; Siddiqui *et al*, 2011).

To further increase the diagnostic yield of biopsies obtained by endoscopy, new FNB needles have been developed with the aim of obtaining a greater proportion of analyzable tissue. So, needles with a reverse bevel, needles with a Fransen tip, or even needles with a fork tip design are on the market(Barresi *et al*, 2018).

The diagnostic accuracy of EUS-FNA can then be further enhanced by Rapid-On-Site Evaluation (ROSE), which consists of an extemporaneous evaluation of the biopsy specimen by a cytotechnician/pathologist directly during the procedure. Although the role of ROSE in daily clinical practice is still hotly debated, some studies have demonstrated improved diagnostic accuracy with this technique (Iglesias-Garcia *et al*, 2014; Koul *et al*, 2018; Schmidt *et al*, 2013).

To further increase the specificity of EUS for solid pancreatic lesions and thus to better characterize them, ancillary techniques such as elastography or the use of intravenous contrast (CE-EUS) can be used.

The contrast agent consists of gas microbubbles (mostly hexafluoride sulfur) with a diameter of about 2.5-7 micrometers that, once injected into the vein, remain inside the vessels and interact with the ultrasound scope, enhancing the vascular signal. The different behavior of solid pancreatic lesions after contrast administration allows the operator to make a more accurate diagnosis. Taking three different diseases of the pancreas such as PDAC, PanNEN and chronic mass-forming pancreatitis as examples, we can see that on B-mode evaluation all of them can appear as a focal solid lesion with

hypoechoic structure and well-demarcated margins. However, after contrast administration, PDAC will show diffuse hypoenhancing, reflecting its poor vascularization, PanNENs will be markedly early hyperenhancing, and chronic mass-forming pancreatitis will tend to be isoenhancing (Dietrich *et al*, 2005; Navina *et al*, 2014; Napoleon *et al*, 2010). Two different meta-analyses have evaluated the accuracy of CE-EUS in the diagnosis of PDAC, showing a pooled 93-94% sensitivity and 88-89% specificity (Gong *et al*, 2012; He *et al*, 2017).

More controversial, however, is the role of elastography (EUS-E), a technique in which the stiffness of a lesion is assessed by the tissue response to compression. Doubts about this technique lie in the fact that it is influenced by many factors, such as the presence of cystic spaces or large vessels near the target lesion. Between 2012 and 2017, 7 meta-analyses were published on the role of EUS-E in solid pancreatic lesions, showing a sensitivity of the technique between 95 and 99 percent and a specificity between 67 and 76 percent (Mei *et al*, 2013; Pei *et al*, 2012; Ying *et al*, 2013; Li *et al*, 2013; Xu *et al*, 2013).

However, the diagnostic role of EUS is not limited to the diagnosis of the type of solid pancreatic lesion, but also allows a prognostic assessment based on the local extent of the neoplasm. Various studies have been published over the years regarding the diagnostic accuracy of EUS in the assessment of vascular infiltration, and three meta-analyses conclude that its sensitivity and specificity vary between 66 and 85% and between 89 and 94%, respectively (Nawaz *et al*, 2013). The data from these studies are highly heterogeneous. This is probably related to the fact that EUS can assess vascular infiltration with extremely different sensitivities depending on the vessels evaluated. In fact, the accuracy is very high, higher than CT-scan or MRI's ones, when the portal vein or superior mesenteric vein is evaluated, but it is greatly reduced, due to inherent technical difficulties, when the arterial side is evaluated, especially the superior mesenteric artery and the celiac trunk.

The evolution of "precision medicine" in pancreatic neoplasms

It is clear from these introductory paragraphs that it is of paramount importance to perform an excellent differential diagnosis of pancreatic neoplasms. Indeed, according to the various published guidelines, the role of EUS is to identify the neoplastic lesion of

the pancreas, provide a cytohistologic diagnosis of the type of neoplasm, and perform accurate local staging of infiltration of adjacent organs and vessels. Moreover, at present, as far as PanNENs are concerned, EUS-guided biopsy could/should provide the appropriate material to establish the grading of the neoplasm by Ki67 assessment.

However, as seen in the previous paragraphs, although EUS is the most accurate diagnostic technique, both in terms of positive and negative predictive values, there are still gaps that do not allow a fully adequate diagnosis of all the required factors. In fact, in terms of pathologic diagnosis, the diagnostic adequacy is about 85-90%, especially in those cases where ROSE is not used, so that in one in 10 patients the diagnosis cannot be made immediately, with the risk of having to repeat the examination. In addition, the staging of neoplasms is extremely effective on the venous side but suffers from reduced sensitivity regarding the arterial side and the evaluation of satellite lymphadenopathies.

When analyzing the role of EUS-FNA in the staging of PanNENs, the situation becomes even more complex. Indeed, since a broad array of treatment options exists for these tumors, their grading stands out as a crucial determinant in therapeutic decision-making, given its strong association with prognosis, overall survival, and reduced disease-free survival.

Recognizing the significance of preoperative grading in forecasting the outlook for patients with PanNENs, various researchers have examined the consistency between the grades determined by endoscopic ultrasound-guided fine-needle aspiration/biopsy (EUS-FNA/FNB) and those confirmed by final postoperative histological examination. However, these studies vary widely in their methodology, including the size of the study population, the type of needle used, the version of the WHO classification system applied, as well as the expertise in EUS and pathology across different centers. Consequently, the reported rates of agreement between EUS-based assessments and surgical findings for the Ki-67 index are remarkably inconsistent, ranging from 54% to 100%. Our group has recently published two papers, a retrospective study and a meta-analysis, which showed that the diagnostic accuracy of EUS in grading is good but not excellent (84% for EUS-FNB and 79% for EUS-FNA), with a quietly high risk of errors (Tacelli *et al*, 2021, 2022).

To overcome these problems, various research groups consisting of gastroenterologists, pathologists, computer scientists, engineers and others have tried

over the years to implement the diagnostic and staging capabilities of EUS by inventing new techniques applicable to this method.

RNA extraction from EUS-FNA/B:

As we navigate through the genomic era and advance in precision medicine, genome sequencing is revolutionizing the approach to diagnosing, classifying, and treating pancreatic ductal adenocarcinoma (PDAC). The analysis of PDAC gene patterns is gaining traction as a means to forecast how patients will respond to chemotherapy and to pinpoint precise molecular targets for developing targeted therapies (Zheng-Lin & O'Reilly, 2021; Casolino et al, 2021; Puleo et al, 2018; Moffitt et al, 2015; Bailey et al, 2016; Collisson et al, 2011). Significantly, most of the insights gained so far have been from genomic studies of tissue from surgical resections. However, this focus on operable cases overlooks the majority of patients who present with locally advanced or metastatic PDAC at diagnosis — a group comprising up to 80%. This skew in sample selection could potentially distort the wider understanding of the disease.

Concurrently, there's a growing body of evidence supporting the influential part played by the tumor microenvironment, or stroma, in the initiation, progression, and treatment resistance seen in PDAC (Masugi, 2022; Neesse et al, 2019). Components of the stromal tissue are increasingly being recognized as both predictive biomarkers and viable therapeutic targets within PDAC.

Beyond the realm of cytopathological examination, EUS-FNA specimens from PDAC have demonstrated their worth, especially for genomic DNA analysis (Habib et al, 2021; Larghi et al, 2020). RNA analysis from EUS-acquired pancreatic samples has not been as extensively pursued, largely due to the challenges in obtaining high-quality, intact RNA — an obstacle arising from the degradation activities of pancreatic RNAases. Nonetheless, successful RNA profiling from EUS-derived PDAC samples has been achieved through various methods including real-time quantitative polymerase chain reaction (RT-qPCR), RNA Sequencing (RNA-Seq), and digital mRNA assessment via NanoString technology (Archibugi et al, 2020; Rasmussen et al, 2021; Lundy et al, 2021). Although the instances of RNA extraction via EUS-guided tissue acquisition (EUS-TA) are limited and the outcomes have been somewhat meager, the potential for valuable insights remains promising. In a first study, only 5–10 ng of RNA were extracted from

EUS-FNA with no report on the integrity and were used for qPCR. Berry et al. reported to retrieve, with one pass of FNA snap frozen in liquid nitrogen, around 12.9 ug of RNA of relatively low quality (mean RIN of 3). The extraction of RNA from archival formalin-fixed paraffin-embedded (FFPE) EUS-FNB samples (therefore requiring at least two or three passes) with a 22G Forktip needle has been recently performed but only 28.8% of samples (n = 45) resulted in being adequate for nanostring analysis and the RNA quality was not reported. In another study, RNA extraction was performed from 40 snap frozen samples acquired through a standard 22G needle, achieving a high quantity of RNA (1 μg) with the quality assessed by agarose gel electrophoresis and spectrophotometry but not quantitatively reported. These samples were adequate to perform a qPCR analysis of the VEGFR genes (Carrara et al, 2021; Berry et al, 2017; Gleeson et al, 2020). As can be seen, both for epidemiological reasons and because of the lethality of the disease, almost all available studies on the possibility of obtaining RNA useful for genomic analysis by EUS-FNA/B are dedicated to PDAC. To date, there are no studies designed to evaluate the possibility of obtaining RNA from PanNENs. As we know, PDAC and PanNEN are two very different tumor types in terms of biological behavior, markers expressed, lethality and vascularization.

Vascularization of PanNENs

Angiogenesis is the formation of new blood vessels from pre-existing ones. This biological process unfolds in four distinct stages, initiating with the release of angiogenic triggers like VEGF under low oxygen conditions, which is then followed by a decrease in the integrity of endothelial cell connections, enhancing vascular permeability. The process proceeds with the endothelial cells migrating, multiplying, and differentiating, which eventually slows as rudimentary capillaries form. The final stage involves the recruitment of supporting cells, such as pericytes and smooth muscle cells, to the nascent vessels. Angiogenesis is a defining characteristic of tumors, essential for neoplasia progression since cancer cells rely on a sufficient blood supply for oxygen and nutrients(Poncet et al, 2009; Couvelard et al, 2008, 2009). Tumors themselves promote vessel formation by secreting growth factors like VEGF and FGF2, fostering capillary growth within the tumor to sustain its expansion. However, the blood vessels formed in tumor angiogenesis are typically abnormal and chaotic, leading to poorly structured

vessels that facilitate not just tumor growth but also metastasis by allowing cancer cells to enter and exit the bloodstream more easily.

NETs are distinguished by their high degree of vascularity (Palazzo *et al*, 2018; Schmitt *et al*, 2009; Cappelli *et al*, 2015; Couvelard *et al*, 2009). They exhibit a microvascular density (MVD) much higher than that of typical carcinomas, sometimes up to thirtyfold greater, resembling the vascular richness of normal glandular tissues, which is vital for the extensive exchange between the blood and endocrine cells.

NETs are also unique in their ability to produce and release substantial amounts of VEGF, which then activates specific receptors on various cells, including endothelial and vascular smooth muscle cells as well as monocytes and macrophages. This VEGF production is closely linked to oxygen levels, increasing under hypoxia by binding to hypoxia-inducible factors like HIF-1, which is normally degraded by the VHL tumor suppressor gene. A mutation in VHL can lead to the constant activation of angiogenesis and subsequent neoplasia due to the continual presence of HIF (D'Assignies *et al*, 2009; Kim *et al*, 2017; Fujino *et al*, 2016).

MVD is widely used to quantify angiogenesis by counting the number of microvessels in a square millimeter of tumor tissue (De Palma *et al*, 2017). However, assessing MVD alone doesn't fully reveal the functional state of a tumor's blood vessels since some neoplasms display lower MVD than even normal tissues, like those in the lung, breast, or colon. Furthermore, not all tumors react uniformly to hypoxia, with some able to endure low oxygen levels without succumbing to cell death. Despite some debate, MVD has been linked to prognosis in various solid tumors, although findings regarding pancreatic cancer remain mixed. Recent meta-analysis does suggest a correlation between high MVD, decreased survival, and increased recurrence post-surgery (Ntellas *et al*, 2019).

In PanNENs, which vary in their degree of aggressiveness and typically showcase dense vascular networks, the relationship between MVD and tumor behavior deviates from other tumor types. Contrary to other neoplasms, a higher MVD in PanNENs often indicates better differentiation and lesser aggression, while a lower vascular density is associated with increased malignancy. This observation, known as the "neuroendocrine paradox," was initially reported in 2003 when it was discovered that higher MVD in PanNENs was linked to smaller tumors, lower proliferation indices, and a reduced metastatic tendency(Scoazec, 2013). Subsequent studies have supported this

counterintuitive finding, suggesting that in NETs, vessel density is more indicative of differentiation rather than aggressiveness.

Artificial intelligence (AI) in EUS

AI is a multifaceted fusion of computer systems and software crafted to create algorithms that demonstrate critical thinking and intelligence. AI's transformative impact on clinical practice is primarily driven by its three key branches: machine learning (ML), artificial neural networks (ANNs), and expert systems (ES). A notable advance in AI is deep learning (DL), a subset of ML (Panch et al, 2018). DL emulates the intricate structure of human brain networks, layering multiple nonlinear processing stages to progressively abstract data. This abstraction allows for sophisticated levels of feature detection and assists in tasks like target detection, classification, or segmentation (Dahiya et al, 2022).

AI has been particularly influential in the field of gastroenterology (GI), enhancing the precision of diagnoses, minimizing errors, standardizing interpretations of radiologic and histopathologic data, and refining intervention planning. The capability of AI to improve diagnostic outcomes is evidenced in endoluminal and pancreaticobiliary disorders. For instance, a retrospective study involving 50 patients with intraductal papillary mucinous neoplasms (IPMNs) utilized EUS imagery for a DL model, yielding high sensitivity, specificity, and accuracy rates for detecting malignancy in IPMNs (Kuwahara *et al*, 2019). Similarly, a systematic review encompassing 11 studies on AI-enhanced EUS in diagnosing pancreatic cancer showed accuracy rates ranging from 80 to 97.5%, sensitivity from 83 to 100%, and specificity from 50 to 99% (Goyal *et al*, 2022).

AI-aided EUS is particularly promising for early screening and diagnosis of pancreatic cancer. The differentiation of pancreatic ductal adenocarcinoma (PDAC) from chronic pancreatitis (CP), which often presents with similar radiological features, is a notable diagnostic hurdle. Since CP can be both a mimic and a risk factor for PDAC, and the two can coexist in a patient, AI models can be crucial for accurate diagnosis (Səftoiu *et al*, 2015; Săftoiu *et al*, 2012; Das *et al*, 2008).

Although EUS imaging is a powerful tool, even specialists may need to supplement it with fine-needle biopsy (FNB) to distinguish malignancies from CP. Many studies support the high accuracy of AI models in differentiating PDAC from benign pancreatic

conditions, yet their widespread adoption is tempered by the limited sample sizes in studies, restricting the data available for training AI models.

Despite the early stage of AI application in diagnostics, these models already contribute significantly to medical decision-making and treatment planning for pancreatic cancer. Nonetheless, clinicians remain cautious about fully integrating AI tools into practice, despite their potential. A key challenge for AI-assisted EUS is the absence of standardized protocols for data collection, processing, storage, and analysis. For AI models to attain high diagnostic precision and broad applicability, the training data must be diverse and comprehensive, encompassing the full spectrum of variables integral to clinical decision-making (Dahiya *et al*, 2022).

AIMS

The primary aim of this thesis is to investigate the role of novel diagnostic techniques applied to endoscopic ultrasound (EUS) for the study of pancreatic neuroendocrine neoplasms (PanNENs) beyond merely morphological and pathological descriptions—what is currently typically performed in daily clinical practice.

To achieve this, the thesis has been structured into three sub-projects:

- Feasibility of RNA Extraction: The purpose of this subproject is to evaluate the feasibility of extracting RNA in sufficient quantity and quality to perform genomic analyses from specimens obtained through EUS-FNA of PanNENs. Additionally, within this project, three methods of RNA preservation and extraction will be compared to determine which technique yields the best material in terms of quantity and quality.
- The Role of EUS in the Assessment of Microvascularization of PanNENs: This subproject has a dual purpose:

(1) To explore the potential for providing a quantitative assessment of contrast uptake by PanNENs during EUS and compare it with the uptake in pancreatic adenocarcinomas.

(2) To assess whether EUS with contrast enhancement (EUS-CE) can predict the microvessel density of PanNENs and its association with the aggressiveness of the neoplasm.

- The Role of AI in Predicting Differential Diagnosis of Pancreatic Neoplasms: The aim of this subproject is to apply deep learning models to images collected during EUS for pancreatic neoplasms to assess the potential for obtaining a differential diagnosis of the tumor's cyto-histological type before performing a biopsy.

RESULTS

RNA extraction

In this prospective sub-project a cohort of 37 PanNEN patients were enrolled, with a slight predominance of male participants (62.2%). The median age at diagnosis was 59 years, ranging from 52 to 67 years. The median Body Mass Index (BMI) was calculated to be 27.16 kg/m^2, with an interquartile range (IQR) indicating variability from 24.9 to 30.3.

When considering lifestyle factors, the majority of the cohort were non-drinkers (70.3%) and non-smokers (59.5%). The median size of the lesions as determined by endoscopic ultrasound examination (EUS) was 25 mm, with an IQR of 13 to 60 mm. Tumors were predominantly located in the body-tail region of the pancreas (73.0%), with fewer cases in the head (21.6%) and rare instances of uncinate process involvement or multifocal disease.

The stiffness of the lesions varied, with most being categorized as rigid (81.1%). In terms of contrast enhancement patterns on EUS, hypoenhancing lesions were less common (21.6%) compared to hyperenhancing (29.7%) and isoenhancing (48.6%) types. Metastases were absent in a significant majority of the cases (81.1%), with liver being the most common site of metastasis when present (8.1%).

Ki67 proliferation index values, estimated via EUS, showed a median of 2% with an IQR of 1-3%. The grading of the tumors was predominantly G2 (62.2%). Basing on some peculiar clinical and/or imaging feature (ki67 value, dilation of the pancreatic duct, vessels infiltration, presence of metastasis, diameter) patients were classified as aggressive or non-aggressive, respectively 43.2 and 56.8% (Table 1).

Variable	Total (N=37)
Age at Diagnosis (years), median (IQR)	59 (52-67)
Gender, n (%)	
- Male	23 (62.2)
- Female	14 (37.8)
Weight (kg), median (IQR)	80 (72-95)
Height (cm), median (IQR)	170 (164-180)
BMI, median (IQR)	27.16 (24.9-30.3)
Ever Drinker, n (%)	
- Yes	11 (29.7)
- No	26 (70.3)
Ever Smoker, n (%)	
- Yes	15 (40.5)
- No	22 (59.5)
EUS Size (mm), median (IQR)	25 (13-60)
Tumor Location, n (%)	
- Head	8 (21.6)
- Body-Tail	27 (73.0)
Lymph Node Involvement, n (%)	
- Present	4 (10.8)
- Absent	33 (89.2)
Lesion Stiffness, n (%)	
- Soft	5 (13.5)
- Rigid	30 (81.1)
Enhancement Pattern, n (%)	
- Hypoenhancing	8 (21.6)
- Hyperenhancing	11 (29.7)
Metastases, n (%)	
- Absent	30 (81.1)

Variable	Total (N=37)
- Liver	3 (8.1)
Ki67 (EUS Estimation), median (IQR)	2 (1-3)
Grading, n (%)	
- G1	5 (13.5)
- G2	23 (62.2)
Aggressiveness Group, n (%)	
- Less Aggressive	21 (56.8)
- More Aggressive	16 (43.2)

Table 1: General features of patients included in sub-project 1

The median global RNA concentration extracted from the lesions was 11,000 pg/ul, with an IQR stretching from 4730 to 19700 pg/ul, and the median RNA Integrity Number (RIN) was 3.7 with a standard deviation of ±1.6, reflecting the variability in RNA quality. Median RNA concentrations were compared across three different extraction methods. Method 1 (Snap Frozen + Trizol) yielded a median RNA concentration of 18,400 pg/µL with an interquartile range (IQR) of 5,295 to 24,550 pg/µL. Method 2 (Fresh tissue plus 1-Thioglycerol buffer solution) resulted in a median RNA concentration of 13,000 pg/µL (IQR 7,820-18,225), while Method 3 (Snap Frozen plus 1-Thioglycerol buffer solution) produced a median concentration of 5,010 pg/µL (IQR 3,745-5,825). The RNA Integrity Number (RIN) was also assessed according to the extraction method used, revealing median RIN values of 3.9 (IQR 3.3-5.7) for Method 1, 2.4 (IQR 1.3-5.7) for Method 2, and 5.0 (IQR 4.45 – 5.7) for Method 3.

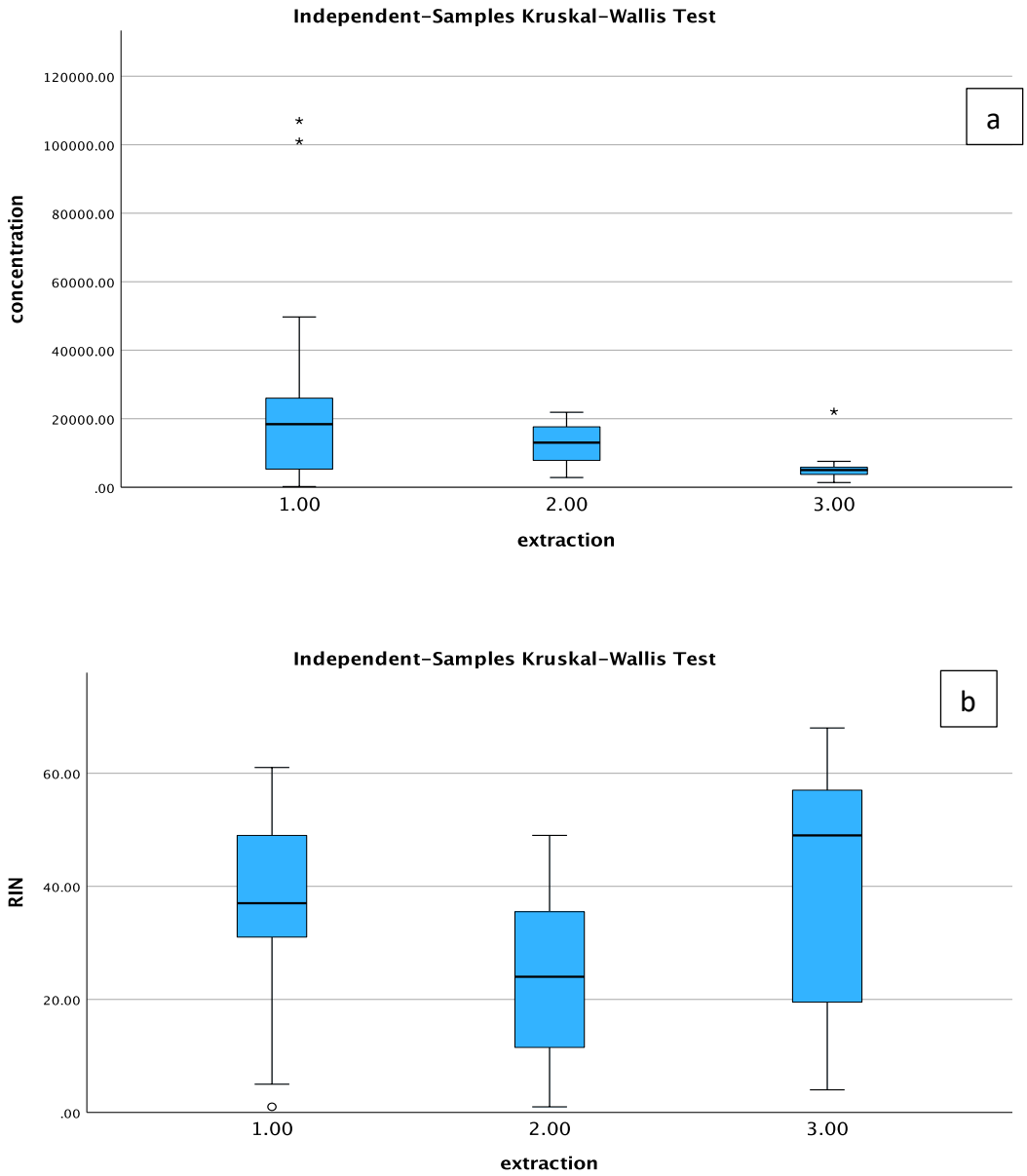

Figure 1: Differences of concentration (a) and RIN (b) according with different RNA extraction Methods

Statistical analysis utilizing the Kruskal-Wallis test demonstrated a significant difference between Methods 1 and 3 (p=0.008) and between Methods 2 and 3 (p=0.024), with no significant difference observed between Methods 1 and 2 (p=0.751). Regarding RIN values, a statistically significant difference was found between Methods 2 and 3 (p=0.02), along with a non-significant trend between Methods 1 and 3 (p=0.064; Figure 1).

A univariate linear regression analysis was conducted to identify potential factors that could influence the quantity and quality of the extracted RNA. The covariates considered included sex, age, BMI, tumor aggressiveness, alcohol consumption, smoking status, lesion diameter, lesion rigidity assessed by EUS elastography (EUS-E), contrast enhancement patterns, presence of metastasis, and tumor grading. This analysis did not reveal any statistically significant associations with RNA concentration or RIN values (Table 2).

Model		Unstandardized Coefficients		Std. Co	t	Sig.
		B	Std. Error	Beta		
CONCENTRATION	(Constant)	78008.681	62001.438		1.258	.234
	Aggressiveness	-35219.305	22276.884	-.696	-1.581	.142
	Sex	-7728.616	17361.871	-.134	-.445	.665
	BMI	-1.022E-5	.000	-.240	-.844	.417
	Alcohol cons.	-12811.054	18531.301	-.231	-.691	.504
	Smoking	-7870.455	16882.878	-.155	-.466	.650
	Diameter	652.985	406.444	.738	1.607	.136
	Location	-11432.597	15100.305	-.198	-.757	.465
	Lymph Nodes	23502.276	27055.945	.407	.869	.404
	EUS-E Rigidity	-9053.459	13949.201	-.201	-.649	.530
	Contrast Enhancement	52721.868	42668.028	.394	1.236	.242
	Metastases	48649.996	26189.147	.800	1.858	.090
	Ki67	-8.670	735.088	-.005	-.012	.991
	Grading	-25170.519	19992.220	-.628	-1.259	.234

R I N	(Constant)	25.092	45.996		.546	.596
	Aggressiveness	-19.977	16.268	-.507	-1.228	.245
	Sex	7.111	12.126	.158	.586	.569
	BMI	2.915E-10	.000	.009	.033	.974
	Alcohol cons.	4.942	13.223	.115	.374	.716
	Smoking	3.450	11.939	.088	.289	.778
	Diameter	.516	.277	.749	1.867	.089
	Location	-1.338	10.880	-.030	-.123	.904
	Lymph Nodes	-3.869	19.626	-.086	-.197	.847
	EUS-E Rigidity	-12.657	9.234	-.361	-1.371	.198
	Contrast Enhancement	16.805	31.604	.161	.532	.605
	Metastases	3.117	21.080	.066	.148	.885
	Ki67	.578	.486	.462	1.187	.260
	Grading	8.860	14.793	.284	.599	.561

Table 2: Linear univariate analysis for possible variables influencing RNA concentration (a) and RIN (b)

Microvascularization assessment

Quantitative Contrast Evaluation:

In this sub-project, after applying inclusion and exclusion criteria, a prospective cohort of 73 patients with focal pancreatic lesions (51 PDACs and 22 PanNENs) was studied. The general characteristics of the study population are summarized in Table 3. No statistically significant differences were observed between the PDAC and PanNENs cohorts regarding the general characteristics under consideration, specifically with respect to age, gender, and lesion size and location.

Variable	Overall n= 73	PC n= 51	PanNEN n= 22
Sex (M)	36 (49)	23 (45,1)	14 (63)
Age (y)	66 (41-95)	67 (51-95)	62 (41-81)
BMI (Kg/m2)	24 (15,7-33,9)	23,7 (15,7-33,9)	24,8 (18,3-31,3)
Smoking	27 (37)	22 (43)	5 (23)
Tumor Location	26 (36)	20 (39)	6 (27)
Diameter (mm)	31 (7-130)	32,6 (10-60)	27,3 (7-130)
Echogenicity (hypo-)	70 (96)	51 (100)	19 (86,4)
Enhancement (Hypo-)	45 (61,5)	44 (88,2)	1 (4,6)
Vanishing pancreas	16 (22)	5 (10)	11 (50)
Chronic pancreatitis signs	2 (3)	1 (2)	1 (4,5)
Lymph nodes	22 (30,1)	19 (37,2)	3 (13,6)

Table 3: Comparison of demographic, clinical and pathological characteristics between patients with PC and PanNEN

Following the analysis of contrast enhancement in endoscopic ultrasound with contrast enhancement (EUS-CE) using Vuebox® software, significant statistical differences were noted between PDAC and PanNENs for the following variables (Table 4): Peak Enhancement (PE) (183.3% for PanNENs vs 26.7% for PDACs; $p<0.001$), Wash-in Area Under the Curve (WiAUC) (2629.96 vs 52.44%; $p<0.001$), Wash-in Rate (WiR) (247.9 vs 35.3%, $p=0.001$), Wash-in Peak Intensity (WiPI) (176.8 vs 26.4%; $p<0.001$), Wash-out AUC (WoAUC) (928.7 vs 47.8%, $p<0.001$) and Wash-in Wash-out AUC (WiWoAUC) (1070.9 vs 42.7%; $p<0.001$).

Variable	PanNEN	PDAC	p-value
MeanLin[%]	111,136	37,14	0,0001
PE[%]	183,34	26,75	<0,0001
WiAUC[%]	2629,96	52,44	<0,0001
RT[%]	514,25	190,8	0,85
mTTl[%]	256,59	320,53	0,72
TTP[%]	583,67	181,59	0,7
WiR[%]	247,86	35,3	0,0011
WiPI[%]	176,83	26,38	<0,0001
WoAUC[%]	928,71	47,8	0,0001
WiWoAUC[%]	1070,9	42,69	<0,0001
FT[%]	247,96	176,28	0,64

Table 4: Differences in Relative Ratio of PanNENs and PDAC contrast medium uptake parameters

A sensitivity analysis was conducted via the construction of a Receiver Operating Characteristic (ROC) curve considering all variables found significant in the univariate Mann-Whitney test. The two parameters with the highest AUC were WiPI (AUC 0.838, 95%CI 0.743-0.933) and WiR (AUC 0.804, 95%CI 0.699-0.910; Figure 2). By combining these variables through logistic regression, we were able to enhance the accuracy of the model to identify PDAC to 96.1%.

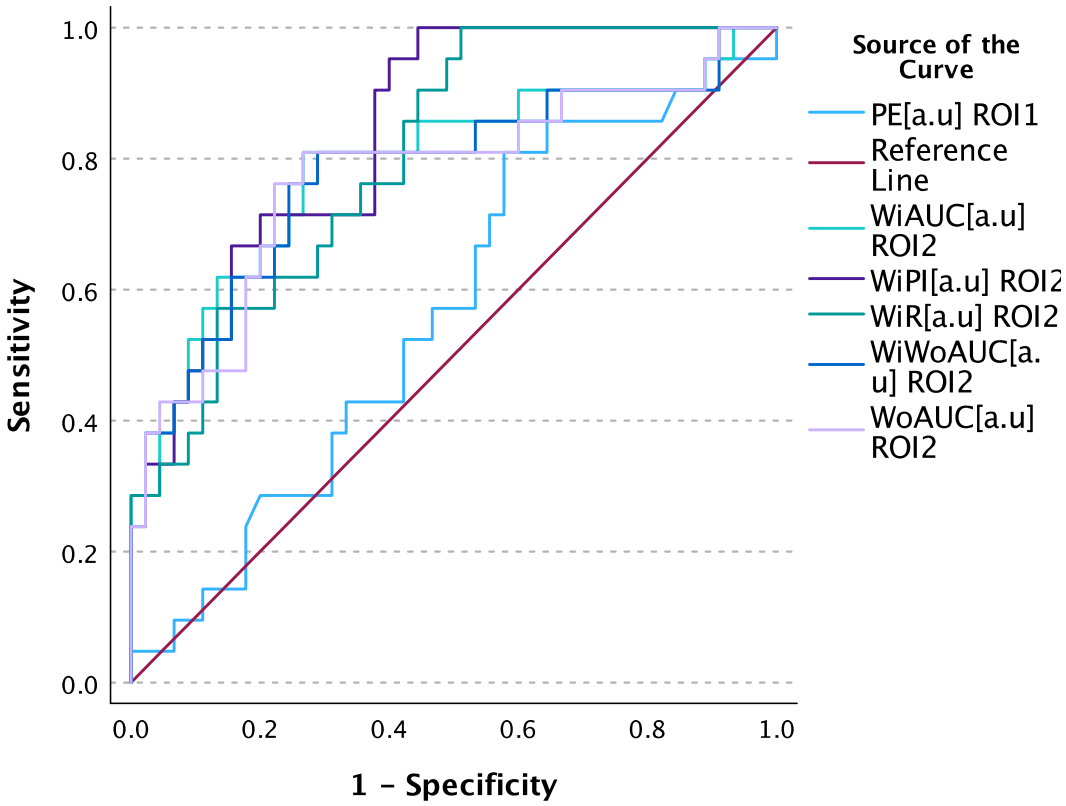

Figure 2: Sensitivity and Specificity of captation parameters in distinguishing PanNENs and PDACs by ROC curve analysis

To identify potential confounding factors that could influence the quantitative parameters of contrast uptake, a univariate logistic regression was performed. In PanNENs, factors significantly associated with variations in the parameters considered were the diameter of the lesion, its echogenicity, and the presence of lymphadenopathy (Table 5a). Multivariate logistic regression analysis retained a statistically significant correlation between the lesion diameter and the average local transit time ($p<0.0001$). A similar analysis was conducted on patients with PDAC; in this case, the variables significantly associated with lesion contrast uptake parameters were a history of alcohol and tobacco use, body mass index, and the location of the tumor (Table 5b). In the multivariate analysis, no patient-level or tumor-level variable remained statistically associated with the contrast uptake parameters.

PanNEN											
	Age	Sex	BMI	Smoking	Location	Diameter	Echogenicity	Enhancement	Vanishing	CP signs	Lymph nodes
MeanLin[%]	0,87	0,95	0,88	0,47	0,99	0,97	0,06	0,44	0,7	0,49	0,29
PE[%]	0,74	0,71	0,05	0,41	0,35	0,28	0,98	0,99	0,6	0,55	0,35
WiAUC[%]	0,66	0,8	0,23	0,65	0,14	0,65	0,78	0,47	0,91	na	0,52
RT[%]	0,7	0,7	0,28	0,38	0,12	0,86	0,78	0,82	0,2	0,64	0,77
mTTI[%]	0,58	0,7	0,42	0,53	0,4	<0,0001	0,18	0,52	0,84	0,56	0,83
TTP[%]	0,73	0,41	0,28	0,32	0,22	0,9	0,83	0,73	0,54	0,75	0,76
WiR[%]	0,27	0,26	0,27	0,54	0,98	0,32	0,67	0,52	0,81	0,62	0,61
WiPI[%]	0,69	0,73	0,07	0,44	0,32	0,28	0,95	0,9	0,64	0,69	0,4
WoAUC[%]	0,69	0,84	0,08	0,51	0,25	0,65	0,74	0,75	0,66	0,33	0,5
WiWoAUC[%]	0,68	0,77	0,07	0,53	0,24	0,66	0,74	0,57	0,3	0,29	0,51
FT[%]	0,75	0,37	0,15	0,23	0,22	0,93	0,7	0,6	0,58	0,45	0,9
WoR[%]	0,22		0,17	0,42	0,6	0,34	0,51	0,9	0,39	0,73	0,18

PDAC											
	Age	Sex	BMI	Smoking	Location	Diameter	Echogenicity	Enhancement	Vanishing	CP signs	Lymph nodes
MeanLin[%]	0,68	0,8	0,56	0,17	0,67	0,67	na	0,74	0,15	0,38	0,36
PE[%]	0,76	0,27	0,58	0,36	0,69	0,47	na	0,9	0,28	0,77	0,47
WiAUC[%]	0,55	0,52	0,49	0,43	0,83	0,97	na	0,95	0,31	0,56	0,56
RT[%]	0,7	0,28	0,82	0,69	0,78	0,59	na	0,89	0,41	0,47	0,17
mTTI[%]	0,47	0,15	0,44	0,8	0,33	0,91	na	0,39	0,54	0,45	0,36
TTP[%]	0,62	0,7	0,24	0,19	0,41	0,85	na	0,17	0,32	0,79	0,21
WiR[%]	0,54	0,16	0,9	0,27	0,45	0,56	na	0,82	0,54	0,98	0,59
WiPI[%]	0,77	0,35	0,82	0,35	0,74	0,4	na	0,94	0,36	0,72	0,28
WoAUC[%]	0,48	0,49	0,21	0,6	0,6	0,85	na	0,77	0,51	0,42	0,48
WiWoAUC[%]	0,97	0,53	0,21	0,67	0,61	0,86	na	0,79	0,45	0,45	0,37
FT[%]	0,7	0,49	0,34	0,5	0,58	0,83	na	0,79	0,55	0,31	0,44
WoR[%]	0,51	0,16	0,25	0,39	0,22	0,56	na	0,82	0,32	0,96	0,62

Table 5: Univariate Logistic Regression Analysis of Contrast Uptake Parameters in PanNENs (a) and PDACs (b) patients

Microvessel Density Assessment

In this segment of the project, 66 patients who underwent surgery for NF-PanNEN and had preoperative Contrast-Enhanced Computed Tomography (CE-CT) and/or CE-EUS were retrospectively enrolled. Their demographic and clinicopathological characteristics are detailed in Table 6. The study group was divided based on Microvascular Density (MVD) using a median value as a threshold to categorize patients into those with high MVD (>165 microvessels/mm^2) and low MVD (<165 microvessels/mm^2). A notably higher incidence of lymph node metastases (N1) was observed in patients with low MVD compared to those with high MVD (61% vs 33%; p= .026).

Variable	Overall	Low MVD	High MVD	p
Sex (m)	37 (56)	17 (52)	20 (61)	0.457
Age (y)	58 (48-65)	59 (48-68)	58 (49-64)	0.708
BMI, Kg/m2*	24 (22-28)	25 (22-27)	24 (21-29)	0.387
Location (head)	31 (47)	15 (45)	16 (48)	0.805
Diameter (mm)	30 (24-40)	30 (25-37)	30 (22-46)	0.648
Stage T (T3-T4)	25 (38)	11 (33)	14 (42)	0.447
Stage N (N1)	31 (47)	20 (61)	11 (33)	0.026
Stage M, M1	10 (15)	6 (18)	4 (12)	0.492
Ki67 proliferative index, %	3.5 (1-8)	6 (2.5-10)	2 (1-5.5)	0.018
Tumor grading				0.024
PanNEN G1	25 (38)	8 (24)	17 (52)	
PanNEN G2	38 (58)	22 (67)	16 (48)	
PanNEN G3	3 (4)	3 (9)	0 (0)	
Microvascular Invasion	38 (58)	24 (73)	14 (42)	0.013
Perineural Invasion	22 (33)	12 (36)	10 (30)	0.602
DAXX, loss	18 (27)	14 (42)	4 (12)	0.006
ATRX, loss	6 (10)	3 (10)	3 (9)	1.000

Table 6: Comparison of demographic, clinical and pathological characteristics at baseline between patients with low tumor and high tumor MVD

Furthermore, a significantly greater proportion of low MVD patients were found to have tumors at an advanced stage (III-IV) (36%; p= .007). The median Ki67 proliferation index was considerably higher in the low MVD group (6% [range 2.5%-10%] vs 2% [range 1%-5.5%], p= .018). Correspondingly, those with low MVD, in contrast to their high MVD counterparts, exhibited a significantly higher prevalence of grade 2/3 tumors

(76% vs 48%, p= .022), microvascular invasion (73% vs 42%, p= .013), and loss of DAXX/ATRX expression (52% vs 21%, p= .011). After a median follow-up of 29 months (interquartile range 20-40 months), disease recurrence was documented in 21% of patients. A trend towards a shorter Disease-Free Survival (DFS) was noted in the low MVD group compared to the high MVD group, with 3-year DFS rates of 67% versus 87%, although this did not reach statistical significance (p= .071).

Out of the cohort, CE-EUS data was available for 37 patients (56%). Those with low MVD demonstrated a significantly increased proportion of arterial hypoenhancement compared to the high MVD group (37% vs 6%, p= .042). Late-phase washout was more commonly observed in the low MVD group (42% vs 11%, p= .034). Consistently, patients with arterial hypoenhancement exhibited a substantially lower MVD compared to those with iso/hyperenhancement (142 microvessels/mm^2 [range 77-151] vs 202 microvessels/mm^2 [range 154-315], p= .021). Similarly, those exhibiting late-phase washout had a lower MVD compared to those with early washout (p= .011).

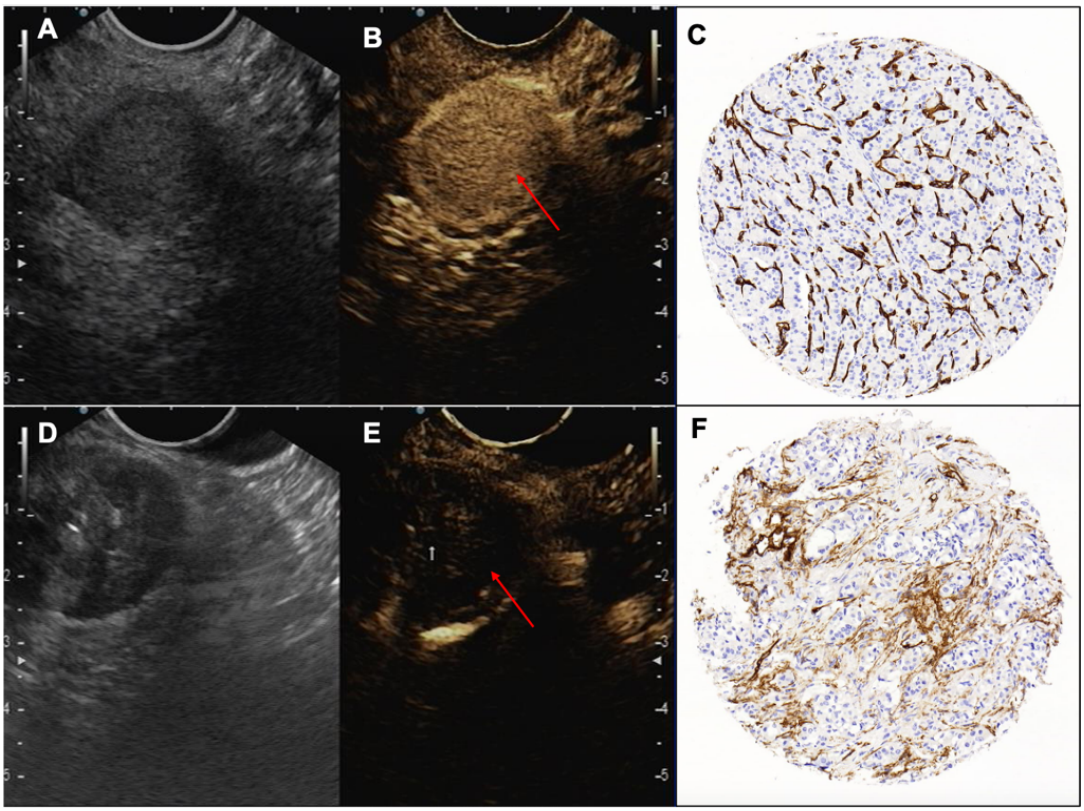

Figure 3: PanNENs with different pattern of arterial enhancement (hyperenhancing - A-D- and hypoenhancing - B-E) after administration of contrast medium, with the corresponding microvascular density (C-F).

Both univariate analysis and multivariate logistic regression were employed to pinpoint predictors of low MVD prior to surgical intervention, with the latter analysis focusing specifically on patients for whom CE-EUS data was available (n=37). In the multivariate logistic regression analysis, late-phase washout emerged as the sole independent predictive factor of low MVD (Odds Ratio 9.545, 95% Confidence Interval 1.021-89.223, p= .048) as indicated in Table 7.

Variable	Univariate analysis		Multivariate analysis	
	OR (95% CI)	***p***	**OR (95% CI)**	***p***
Sex Male Female	1 0.917 (0.243-3.463)	0.898		
Age < 60 years ≥ 60 years	1 0.886 (0.247-3.341)	0.886		
BMI < 25 Kg/m^2 ≥ 25 Kg/m^2	1 1.143 (0.299-4.367)	0.845		
Tumor grading G1 G2-G3*	1 3.439 (0.887-13.259)	0.074		
Stage I-II III-IV	1 4.400 (1.041-18.599)	**0.044**	–	–
Arterial Enhancement Hyper-enhancement Hypo-enhancement	1 9.917 (1.075-91.469)	**0.004**	–	–
Washout Early Late	1 5.818 (1.032-32.793)	**0.046**	1 9.545 (1.021-89.223)	**0.048**

Table 7: Univariate and Multivariate Logistic Regression Analysis to Predict Low Microvascular Density in Patients Undergoing CE-EUS

EUS-AI models in the prediction of differential diagnosis of pancreatic neoplasms

The analytical capabilities of two distinct artificial intelligence models applied to endoscopic ultrasound (EUS) images for the diagnosis of solid pancreatic neoplasms were evaluated, particularly for differentiating Pancreatic Ductal Adenocarcinoma (PDAC) from Pancreatic Neuroendocrine Neoplasms (PanNENs). The dataset comprised 307 de-identified images, including 106 PanNENs and 201 PDAC, categorized into training (60%), validation (20%), and test sets (20%). The demographic and clinicopathological characteristics of patients included in the analysis are detailed in Table 8.

	PanNENs	**PDAC**	**TOTAL**
Sex (M)	58.39%	51.79%	55.74%
Median age at diagnosis (y)	58.65 y IQR (50.64 – 68.05)	69.5 y IQR (61,75-75)	64 y IQR (54-73)
Median lesion size (mm)	18 mm IQR (13 – 28)	37.5 IQR (27,25-44)	29 IQR 24 (16-40)
Multifocal	10.1%	0	5.5%
Median Ca19.9 (U/ml)	/	198.3 IQR (62 – 887.75)	
Median Ki67%	Median Ki67 2%, IQR (1 - 4)		
Grading	G1 81.2% vs G2-G3 18.79%		
Functioning	9.06%	/	
Metastasis at diagnosis	14.8%	23.1%	22.7%
Metastasis location	Liver 8.1%, Lymph Nodes 9.40%, Other 1.7%	Liver 15.1% Lymph nodes 5.2% Other 11.5%	Liver 11.3% Lymph Nodes 7.5% Other 6.2%
Surgery	38.4%	27.1%	38.4%
Median follow up (months)	27.5 IQR (12 – 41,25)	14 IQR (10-20)	18 IQR (10-31)

Table 8: demographic and clinicopathological characteristics of patients included in the sub-project 3

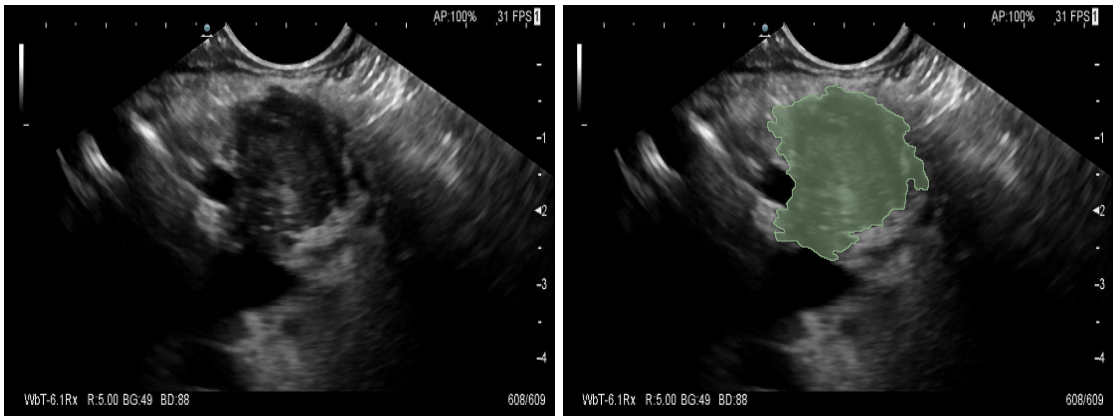

Figure 4: Example of segmentation of a EUS image of a PDAC

Model 1, which executed both classification and lesion segmentation, yielded an average precision in classification of 87.48% with a standard deviation (SD) of 4.61%, an ROC AUC of 80.12% ± 2.97%, balanced accuracy of 71.00% ± 5.42%, a specificity of 60.00% ± 10.96%, and a sensitivity of 82.00% ± 5.42%. The segmentation performance of Model 1 was evaluated with an Intersection over Union (IOU) metric, resulting in a mean IOU of 53.65% with an SD of 2.52%.

Model 2, focused solely on the classification task, outperformed Model 1 slightly in this domain. The average precision was recorded at 88.90% ± 4.48%, with a ROC AUC of 82.00% ± 5.78%. The balanced accuracy was moderately higher than Model 1, at 73.63% ± 4.95%. Furthermore, Model 2 demonstrated an increase in specificity to 64.76% ± 9.28% and maintained a comparable sensitivity of 82.50% ± 11.18%. In summary, while both models demonstrated robust diagnostic potential, Model 2 exhibited enhanced precision and balanced accuracy for the classification of PDAC versus PanNENs.

DISCUSSION

RNA extraction

In this sub-project of the PhD thesis, we have ventured into the uncharted territory of RNA extraction from EUS-FNA in patients with PanNEN. The contemporary clinical landscape, as outlined by current guidelines, primarily utilizes cyto-histological samples obtained from EUS-FNA for PanNENs to conduct pathological investigations. These typically include the identification of the lesion type through hematoxylin-eosin staining or immunohistochemical analysis with antibodies targeting specific antigens such as chromogranin or synaptophysin. Moreover, PanNENs stand out as the sole tumors for which EUS-guided biopsy results can establish a risk of aggressiveness and progression, tied to the biological and oncological behavior of the neoplasm related to the percentage expression of Ki67, hence the grading(Dasari *et al*, 2017; Klöppel *et al*, 2017; Rindi *et al*, 2012b). Indeed, tumors with a lower grading often have an indolent prognostic course, even in cases with distant metastases at diagnosis, while those with higher grading or poor histological differentiation are aggressive and may mirror the behavior of infiltrating PDAC.

Grading, underpinned by the accurate assessment of Ki67 through EUS-FNA, remains the gold standard for proper staging of PanNEN patients and is crucial for therapeutic decision-making, ranging from periodic follow-up to surgery and medical therapy, including chemotherapy. However, two articles recently published by our group have highlighted that the diagnostic accuracy of EUS in grading is commendable but not without faults, with a considerable risk of error(Tacelli *et al*, 2022, 2021). Additionally, for some patients, the EUS-FNA specimens may contain enough cells for diagnosis but not for immunohistochemical analysis. Moreover, the potential heterogeneity within PanNENs suggests that different areas of the same lesion might exhibit different grading values, indicating that a single biopsy may not truly represent the lesion's overall aggressiveness(Couvelard *et al*, 2009).

This sets the stage for surpassing current risk stratification methods by adopting emerging innovative techniques, a challenge this thesis has embraced. We have sought to identify alternative methodologies applicable to endoscopy, such as deep learning

models, direct RNA analysis from primary tumor biopsies at diagnosis, and microvascularization study.

The RNA extraction sub-project has broken new ground for PanNENs. As highlighted in the introduction, genomic evaluations on samples from EUS-guided biopsies are not entirely novel but have predominantly focused on ductal adenocarcinoma(Gleeson *et al*, 2020; Berry *et al*, 2017; Carrara *et al*, 2021; Archibugi *et al*, 2020). Few studies have addressed the extraction of RNA specifically from EUS-FNA performed on PanNENs, and none have acknowledged the marked differences between PanNENs and PDAC in terms of oncological cell types, vascularization, and peritumoral infiltration.

This study's median RNA concentrations indicate that while Method 1 (Snap Frozen + Trizol) garnered the most RNA, Method 3 (Snap Frozen plus 1-Thioglycerol buffer solution) displayed significantly higher RIN values, suggesting superior RNA integrity. This key observation underscores the need to understand which extraction techniques on PanNENs provide RNA of the greatest quantity and quality.

One limitation of this sub-project is the exclusive use of cytology needles. Our protocol has relied solely on 25 Gauge needles, designed to yield a sample adequate for cytological analysis. Recent advancements have brought forth needles with "fork" or "shark-tip" designs, capable of garnering fragments suitable for histological examination. It's conceivable that using larger gauge needles designed for histological sampling could yield greater quantities of RNA for genomic analyses, an aspect that future prospective studies on a larger patient cohort could evaluate.

The implications of this study for molecular medicine are profound. The ability to obtain high-quality RNA from EUS-FNA/B of PanNENs paves the way for molecular profiling, enhancing our understanding of these tumors and informing targeted therapeutic strategies. It aligns with oncology's current trajectory, where molecular characterization of tumors is increasingly guiding treatment decisions and prognostic assessments.

In summary, the exploration of RNA extraction from PanNENs via EUS-FNA/B in this study has laid a crucial foundation in precision medicine. It has not only demonstrated the feasibility of this undertaking but also the critical considerations necessary for method selection, setting the stage for future research that could potentially transform the diagnostic and therapeutic landscape for patients with PanNENs.

Microvascularization assessment

In this investigation, we explored the vascularization of pancreatic neuroendocrine neoplasms (PanNENs) through imaging and its correlation with microvascular density (MVD), traditionally studied via tissue samples. Historically, the ability of imaging to delineate vascularization patterns in PanNENs has not been extensively examined. Preoperative description of MVD in PanNEN patients could enhance the understanding of tumor aggressiveness, potentially guiding treatment decisions, especially for those not eligible for surgery. To date, only a handful of studies have assessed PanNEN vascularization via imaging, and its correlation with MVD has been explored in a limited number of series. In this thesis, the vascularization detected through imaging was compared with histopathological evaluation of MVD using CD-34 staining.

A low MVD was significantly associated with aggressive features such as lymph node metastasis, advanced disease stage, Ki67 proliferation index, microvascular invasion, and loss of DAXX/ATRX. There was also a trend towards reduced disease-free survival (DFS) in patients with low MVD compared to those with high MVD, although this was not statistically significant due to a limited number of events. Nonetheless, these findings underscore the importance of MVD in relation to tumor aggressiveness.

This study also investigated the correlation between vascular characteristics on contrast-enhanced endoscopic ultrasound (CE-EUS) and MVD. Low MVD was strongly associated with arterial hypo-enhancement and delayed washout. Only two studies in the literature have reported a significant correlation between early arterial enhancement patterns on CE-EUS and tumor aggressiveness. However, the correlation between the timing of washout on CE-EUS and MVD has not yet been explored. Many studies suggest

that more aggressive PanNENs, besides being less vascularized, are also more fibrotic, leading to the accumulation of contrast medium within the extracellular fibrotic matrix (Scoazec, 2013; Kim *et al*, 2017; D'Assignies *et al*, 2009; Palazzo *et al*, 2018). Additionally, in PanNENs with low MVD, microvessels are typically dilated, indicating reduced blood flow. Mouse model studies have described varying microvascular permeability in more aggressive PanNENs.

Thus, more aggressive PanNENs with low MVD typically appear as heterogeneous, hypo-enhancing lesions with delayed washout. Supporting this, the current study demonstrated that delayed washout on CE-EUS is an independent predictor of low MVD.

Addressing the lack of an objective assessment the enhancement during CE-EUS, a study was conducted on patients with focal pancreatic lesions (PC and PanNEN). After a quantitative analysis of contrast uptake in pancreatic focal lesions on CE-EUS using a dedicated software (Vuebox®), we observed a significant association between wash-in and wash-out under the curve and tumor echogenicity (hyper-/hypoechoic). This may suggest that the echogenicity might reflect a different stage of neoangiogenesis, and consequently of tumor differentiation.

Furthermore, supporting this latter hypothesis, we found a statistically significant association between some vascularization factors analyzed by the software (mTT, TE, and RT) and the presence of local metastatic lymph nodes in PanNEN. This could confirm that a different aggressiveness of the PanNEN could be represented by the vascularization status and this could be evaluated quantitatively by EUS-CE.

Another significant finding is that none of the patient-level variables considered were correlated with the degree of contrast uptake, which could indicate that when assessing tumor vascularization using CE-EUS, what we observe is truly linked to the tumor angiogenesis process, without the influence of external factors such as BMI or patient age.

While it is well known that PC and PanNEN are two lesions characterized by different vascularization and consequently different contrast behavior, the quantitative assessment of enhancement during CE-EUS is an objective parameter that is still lacking in literature today.

Through this analysis, we provide for the first time data that in the future could play an important role in the early stratification of lesions, in evaluating the response to therapy, and possibly guiding therapeutic choices.

Then, it is intriguing to think that the microvascular pattern could be assessed precisely by EUS-CE and so that the choice of antiangiogenic therapy could be guided by this diagnostic exam. Further prospective studies with higher sample sizes and follow up time are encouraged.

This study, however, has some limitations that must be recognized. The main limitation is that it is mostly a retrospective study, so the endoscopic data were extracted after reviewing all cases and the sample size is low.

In the near future, after this proof-of-concept sub-study, it will be interesting to correlate the objective parameters obtained using Vuebox with the immunohistochemical quantification of MVD in a larger and multicenter cohort of patients.

EUS-AI models in the prediction of differential diagnosis of pancreatic neoplasms

The proficiency of Endoscopic Ultrasound (EUS) in the diagnosis of pancreatic neoplasms has been corroborated through numerous studies, positioning it superior to other imaging techniques such as CT, MRI, and transcutaneous ultrasound—especially for smaller lesions. Despite this, the traditional EUS methodology has limitations, and advancements in EUS-FNA/B have significantly improved the promptness and precision of diagnoses, which is crucial for timely treatment. Nevertheless, there remains a discernible deficit in the prognostic evaluation capabilities of EUS, particularly for pancreatic neoplasms.

The concept of radiomics has revolutionized clinical research, notably in oncology, prompting interest in applying artificial intelligence (AI)—broadly encompassing

machine learning and deep learning models—to EUS. Our study ventured into previously uncharted territory by applying deep learning models to EUS in the context of PanNENs, a focus that has been largely absent from the literature to date. We have observed that the morphological aspect in EUS, without the use of ancillary techniques and relying on post-hoc analysis of EUS images alone, can differentiate the cytological diagnosis of a pancreatic focal lesion (PanNEN vs PDAC) through AI models, potentially eliminating the need for potentially risky biopsies.

Our model predicted diagnoses with a notable average precision of 88.9%, opening a future scenario where cytological or histological diagnoses could be made based solely on EUS images and videos. However, the specificity of our model for Model 2 was modest at 64.76%, likely due to our inclusive approach to consecutive PanNENs patients at diagnosis. We intentionally included both indolent small non-functioning NETs with G1 grading and large, poorly differentiated metastatic PanNENs to avoid selection biases that could compromise the translatability of our results to clinical practice. Although not exceedingly high, we believe that specificity could surpass 90% in the future by including data from ancillary EUS techniques, such as detective flow imaging (DFI), contrast medium, or elastography, in our analyses.

Despite numerous publications on AI in medicine(Dahiya *et al*, 2022), almost none have become part of daily clinical practice. This warrants reflection on the reasons behind this lag. One significant barrier is the absence of standardized data collection and analysis protocols for AI algorithms, and the diversity of imaging subsets that different AI models may require. Moreover, most current studies derive data from single institutions, introducing information bias due to lack of dataset diversity. To enhance diagnostic precision and applicability, AI models must be trained on diverse data that encapsulate all the variables relevant to clinical decision-making.

The focus of future studies should be on overcoming these challenges through prospective, multicentric research involving a broad spectrum of professionals, including engineers, data scientists, and medical specialists. A novel approach, yet to be adopted in published studies, is the combination of data. Just as a patient and their disease are

constituted by various puzzle pieces—exposome factors, genetic variability, laboratory tests, radiological and nuclear medicine investigations, histological exams, and more—AI models should evolve to comprehend and integrate all these variables in patient studies.

Thus, the future direction of my research will be aimed at developing AI models that can synthesize this comprehensive array of patient data, reflecting a holistic approach to precision medicine and patient care.

METHODS

EUS procedure

EUS procedures were conducted under deep sedation using Propofol (Diprivan®, Zeneca, Germany) administered intravenously. The procedures were performed with a Pentax therapeutic linear echoendoscope (EG3870UTK, EG38J10UT) and Hitachi ultrasound systems (Arietta 850, Arietta V70) by skilled endoscopists who carry out more than 500 EUS procedures annually.

Patients were preliminarily assessed by an anesthesiologist using a medical history questionnaire and routine blood tests—including complete blood count, liver function tests, renal function, and coagulation studies—to ensure the patient's clinical conditions were compatible with the EUS procedure. All patients provided written informed consent for the EUS, any potential biopsy, and the deep sedation. The EUS was executed by examining the targeted pancreatic neoplastic lesion in B-mode, as well as utilizing supplementary ancillary techniques such as Doppler and intravenous contrast medium (EUS-CE) to investigate the micro- and macrovascularization of the lesion and possible vascular infiltration, and elastography (EUS-E) to assess the lesion's stiffness. Additionally, during each procedure, scans of the remaining pancreas were performed to detect synchronous neoplasms, lymph node stations for potential lymphadenopathies, and the left hepatic lobe for potential hepatic metastases.

The contrast-enhanced EUS (CE-EUS) technique involves the peripheral vein administration of a microbubble ultrasound contrast agent that traverses the lung circulation and causes vascular system contrast enhancement, driven by the microbubbles' oscillation within the ultrasound field. A stable image of the neoplastic lesion was maintained. The software was configured in a CHI mode, typically with an alternate setting, displaying the contrast image on the right side and a grayscale image on the left. A low Mechanical Index (MI) of below 0.2 was chosen. Following careful image stabilization, SonoVue (sulfur hexafluoride, Bracco Pharmaceuticals, Milan, Italy) was injected (4.8 ml) through a peripheral vein. Two distinct phases were identified for pancreatic imaging: an early (arterial) phase (commencing roughly between 10 seconds and 30 seconds) and a venous (late) phase (beginning roughly between 30 seconds and 120 seconds). The procedures were documented, and videos of the EUS-CE were archived in DICOM format.

Sub-projects design

- Feasibility of RNA Extraction: prospective observational monocentric
- Microvascularization assessment:
- Quantitative contrast evaluation: prospective observational monocentric
- Microvessel Density: retrospective observational monocentric
- Diagnostic AI prediction: retro/prospective observational monocentric

RNA extraction

The study was conducted upon the approval of Internal Review Board (IRB BIOGASTRO/2011 updated on 06/11/2017). The assessment of lesion size and characteristics was carried out through the stomach or the duodenal bulb and second portion, contingent on the lesion's site. The selection of the EUS-TA (endoscopic ultrasound-guided tissue acquisition) site was based on achieving the most stable position with the lesion nearest to the ultrasound probe and ensuring an optimal angle for needle insertion, particularly in areas without intervening blood vessels, as determined by Color Doppler imaging.

A single needle type, the 25-gauge Expect Slimline® (Boston Scientific), was utilized for all fine-needle aspirations (FNAs), applying the slow-pull technique. The initial EUS-TA aimed for diagnostic clarity, expressing the obtained tissue onto a glass slide for analysis. At least two smears were prepared per procedure, fixed in 100% alcohol, and stained with hematoxylin and eosin using standard protocols. An on-site cytopathologist evaluated these smears immediately to determine the sample's adequacy and to provisionally classify the lesion as benign, suspicious, or malignant, based on established pathological criteria such as tissue structure, chromatin pattern, cellular and nuclear pleomorphism, the presence of giant cells, and the nuclear-to-cytoplasmic ratio. If the first pass did not yield adequate results, a second attempt was made. Should adequacy still not be achieved, the patient was removed from the study.

If the sample was adequate and malignancy was suspected, an additional pass with the 25G FNA needle was carried out. Samples were then preserved using one of three methods:

- Snap frozen plus Trizol: Specimens were immediately frozen on dry ice and later mixed with Trizol (Invitrogen®, ThermoFisher), then stored at -80°C. Chloroform was added, and after centrifugation, RNA was isolated from the aqueous phase and mixed with ethanol. RNA purification was conducted using the RNeasy Plus Mini Kit (Qiagen®, Germany), resulting in RNA dissolved in RNase-free water.
- Fresh tissue plus 1-Thioglycerol buffer solution: Fresh samples were placed into collection tubes containing a 1-Thioglycerol and BL Buffer solution from the ReliaPrepTM RNA Cell Miniprep System (Promega Corporation, USA). Isopropanol was added, and after vigorous mixing, RNA extraction was completed using the kit's minicolumns. The resultant RNA was again suspended in RNase-free water.
- Snap frozen followed by 1-Thioglycerol buffer solution: Specimens were first snap-frozen and later thawed and processed in the same manner as the fresh samples, following the 1-Thioglycerol buffer protocol.

The integrity and concentration of RNA were measured using the 2100 Bioanalyzer with the RNA 6000 Pico kit (Agilent Technologies, Germany).

Microvascularization assessment

(1) *Quantitative Contrast Evaluation*: This sub-project included all patients who consecutively underwent EUS at the San Raffaele Hospital's biliopancreatic endoscopy unit in Milan from June 2022 to January 2023 and received a final cytological diagnosis of PDAC or PanNENs. The study proceeded after approval from the Internal Review Board (IRB TAILOR-EUS – 13/06/2022). The endoscopic procedure was conducted as described in the "EUS procedure" section. All patients were injected with 4.8 ml of intravenous contrast medium (SonoVue, Bracco Pharmaceuticals, Milan, Italy), and the video was recorded in DICOM format from the moment of injection until 120 seconds after the start, to study both the early arterial phase and the late venous phase. The endoscopist had to maintain a stable, as fixed as possible, position on the target lesion throughout the video, while also keeping the adjacent normal parenchyma in view. Patients whose respiratory movements were too broad to keep a stable view on the target lesion or who needed to evaluate multiple parts of the pancreatic gland during the CE-EUS were excluded from the study. After the procedure, the DICOM videos were analyzed with commercial software (VueBox®, Bracco Suisse SA, Geneva, Switzerland) that processes CE-EUS procedure videos and provides numerical outputs indicating different parameters related to contrast medium uptake. The parameters assessed by the software are as follows:

a. PE: Peak enhancement
b. WiAUC: Area under the curve during Wash-in
c. RT: Rise time
d. mTT: Mean transit time
e. TTP: Time to peak
f. WiR: Wash-in rate
g. WiPI: Wash-in perfusion index
h. WoAUC: Area under the curve during Wash-out
i. WiWoAUC Wash-in and Wash-out AUC – AUC Wash-in e Wash-out

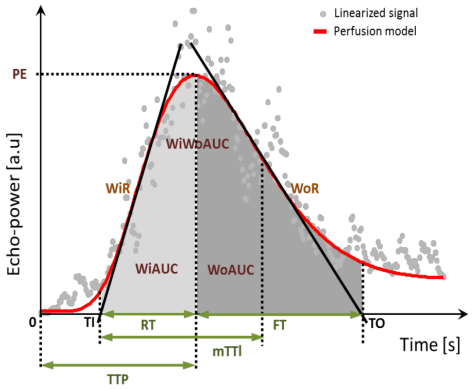

PE	Peak enhancement - Picco di enhancement	[a.u]
WiAUC	Wash-in Area Under the Curve - Area sotto la curva (Wash-in) (*AUC (TI:TTP)*)	[a.u]
RT	Rise Time – Tempo di Innalzamento (*TTP – TI*)	[s]
mTTI	mean Transit Time local - Tempo di transito medio locale (mTT – TI)	[s]
TTP	Time To Peak - Tempo al picco	[s]
WiR	Wash-in Rate - Velocità di Wash-in (*inclinazione massima*)	[a.u]
WiPI	Wash-in Perfusion Index - Indice di perfusione Wash-in (*WiAUC / RT*)	[a.u]
WoAUC	Wash-out AUC - AUC Wash-out (*AUC (TTP:TO)*)	[a.u]
WiWoAUC	Wash-in and Wash-out AUC - AUC Wash-in e Wash-out (*WiAUC + WoAUC*)	[a.u]
FT	Fall Time - Tempo di Caduta (*TO – TTP*)	[s]
WoR	Wash-out Rate - Velocità di Wash-out (*inclinazione minima*)	[a.u]
QOF	Quality Of Fit between the echo-power signal and *f(t)* - Qualità del fitting matematico fra segnale echo-power e *f(t)*	[%]

Figure 5: Captation parameters evaluated by Vuebox software

For analysis, two experienced echoendoscopists manually selected an ROI delineating the image on healthy pancreatic parenchyma and an ROI encompassing the largest assessable surface area of the focal lesion under examination. This software facilitates the evaluation of two types of variables: those pertaining to the quantity of contrast medium, measured by the brightness of individual pixels and expressed in arbitrary units (a.u.), and those concerning the transit time of the contrast, which are denoted in seconds. To normalize any variations that may occur from one examination to another, the contrast uptake values of the lesion were all calibrated relative to those of the adjacent normal parenchyma.

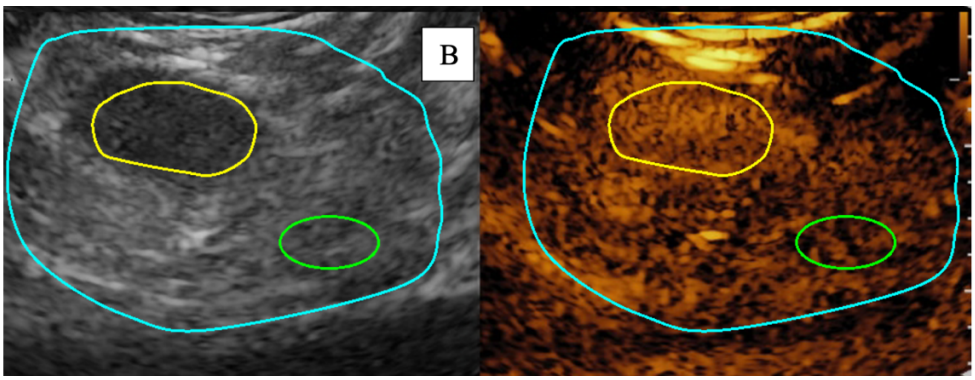

Figure 6: example of ROI delimitation. The PanNEN and normal parenchyma are delimited respectively by the yellow and the green line

(2) *Microvessel Density Assessment*: This study was conducted in collaboration with the Pancreatic Surgery and Radiology units of San Raffaele Hospital. In this cohort, patients who underwent surgery for NF-PanNEN at San Raffaele Hospital between 2016 and 2020 and had a preoperative CE-EUS available were retrospectively evaluated. Patients with functional NETs or poorly differentiated (NEC) were excluded. Clinical data such as age, sex, body mass index (BMI), diagnosis, and preoperative treatment were considered for each patient.

Pathological characteristics were also considered, including the location of the neoplasm (head vs. body-tail), tumor size (maximum diameter on surgical specimen), TNM, tumor grading, microvascular and perineural invasion, presence of necrosis, resection margin status, and the presence or absence of DAXX/ATRX mutations.

The Ki67 proliferation index was defined based on the percentage of MIB1-positive nuclei out of 2000 cells in the hotspot. Grading was assessed according to the 2017 WHO classification into G1 (Ki67<3%), G2 (Ki67 3%-20%), and G3 (Ki67>20%).

Tumor staging was determined in accordance with the current TNM system of the European Neuroendocrine Tumor Society (ENETS). Tissue samples from patients with histologically confirmed diagnosis of NF-PanNEN were subjected to immunohistochemistry with class II CD-34 antibody (1:100, Dako, Glostrup, Denmark; M7165). MVD was calculated by manually counting the number of microvessels per tumor punch based on CD-34 staining. MVD was then expressed as the number of microvessels per 1mm^2. The median MVD (165 microvessels/mm^2) was used to categorize high (>165 microvessels/mm^2) or low (<165 microvessels/mm^2) MVD. Preoperative tumor vascularization assessment was carried out through CE-CT (not part of this PhD thesis) or CE-EUS. CE-EUS data were extracted after case reviews by two experienced echoendoscopists. The arterial enhancement pattern was defined as iso/hyper-enhancing compared to hypo-enhancing. Enhancement was then characterized as homogeneous if there was uniform enhancement within the lesion or otherwise as heterogeneous. The washout timing (early or late) was also reported.

EUS-AI models in the prediction of differential diagnosis of pancreatic neoplasms

The sub-project delineated in this section represents a study conducted in partnership with the Institut de Chirurgie Guidée par l'Image (IHU) in Strasbourg, France. A legal agreement facilitated the sharing of de-identified patient data and echo-endoscopic images, assuring patient confidentiality. Retrospectively, this study encompassed all patients who underwent EUS-FNA at the bilio-pancreatic endoscopy unit of San Raffaele Hospital for solid pancreatic neoplasia from 2018 to 2022. The inclusion criteria were narrowed to patients with cytological diagnoses of Pancreatic Ductal Adenocarcinoma (PDAC) or Pancreatic Neuroendocrine Neoplasms (PanNENs), thereby excluding those with lymphoma, intrapancreatic spleen, serous cystadenoma with pseudo-solid variant, acinar adenocarcinoma, pancreatoblastoma, and solid pseudopapillary tumor. Clinical variables collected included age, sex, symptoms, smoking and alcohol consumption habits, and CA 19-9 levels, along with tumor-related factors such as location, size, multifocality, grading, and presence of distant metastases. Any procedures performed during follow-up or post-therapeutic treatment were omitted from the study. Due to the epidemiological disparity between PanNENs and PDAC, a 1:1 matching based on sex, age, and lesion size was conducted.

For the initial diagnosis, all EUS images were collected and rigorously evaluated by two expert endosonographers, each with over 3000 EUS procedures to their credit. For each case, a single B-mode image that best represented the neoplasm was chosen. Images with Doppler signals or measurement markings were excluded to avoid introducing noise into the model’s input data. An experienced endosonographer (MT) performed the annotation task, delineating the exact morphology and contours of the PanNENs/PDAC lesions using the open-source software 3D-Slicer Version 5.4. Segmentation labels were defined as NET and PDAC. These curated and segmented images were then transferred to the CAMMA (Computational Analysis and Modeling of Medical Activities) research group in Strasbourg for further processing.

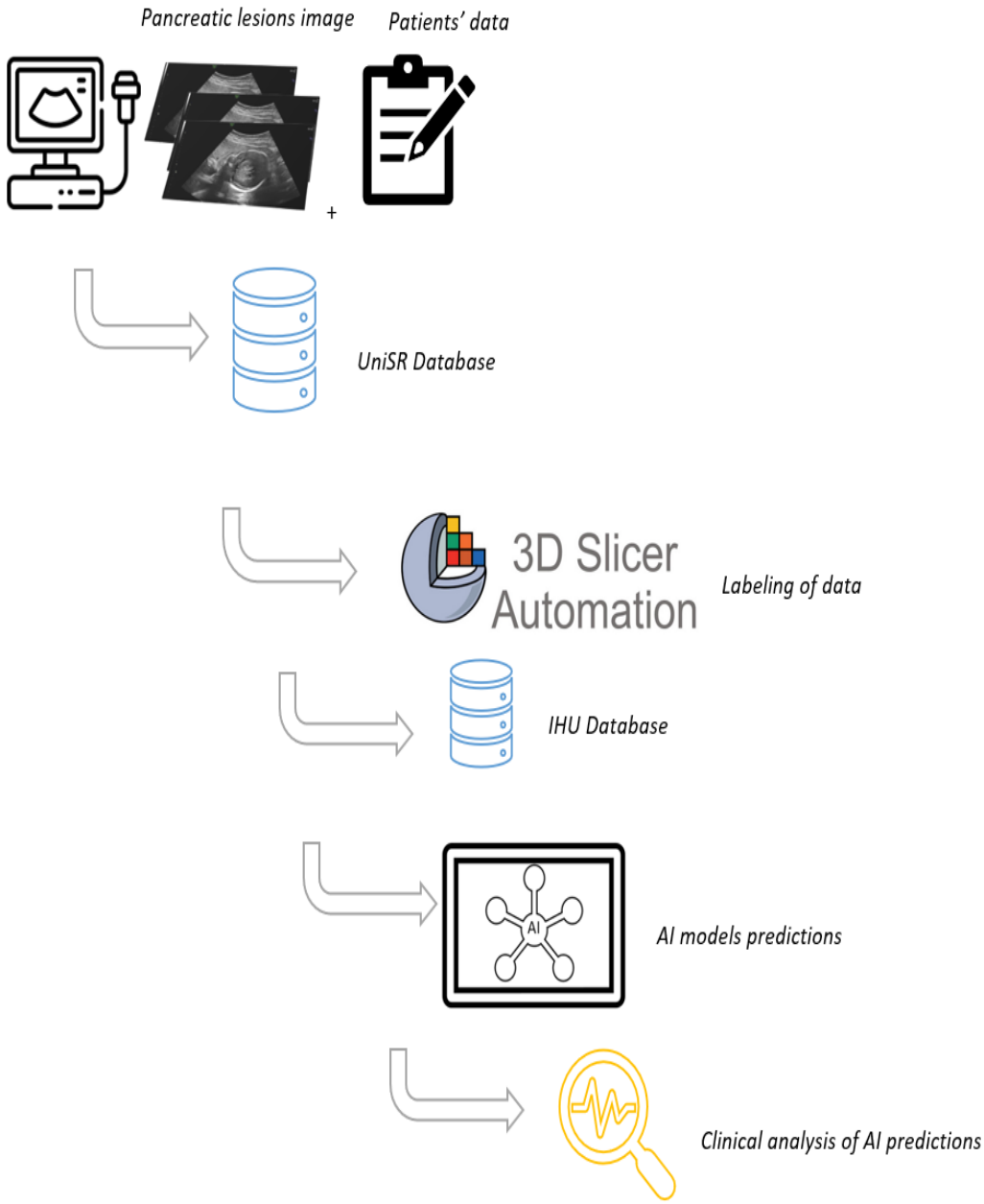

Figure 7: Workflow of data and AI processing

Two distinct models were developed for the task:

1. **Model 1:**

   - This model was designed to perform both NET vs PDAC classification and lesion segmentation.

- The architecture leveraged was Unet, with a specific variation known as R2U-Net, which has shown proficiency in medical segmentation tasks.
- The Unet architecture possesses a bottleneck that houses a compact representation of input features, from which the model predicts the class (NET=0/ PDAC=1).
- The composition of the network layers included input normalization, R2U-Net, a flatten layer, and a dense layer with sigmoid activation, culminating in dual outputs for class and segmentation predictions.
- Data augmentation comprised random rotations (up to 30 degrees) and horizontal flips.
- Hyperparameters were tuned with the Adam optimizer, a combination of cross-entropy and IOU loss functions, a learning rate of 1e-05, a batch size of 16, label smoothing of 0.5, and a maximum of 1000 epochs with early stopping based on validation loss.

2. **Model 2:**
   - This model focused solely on the classification of NET vs PDAC.
   - The architectural base was the VGG16 model, adhering to the normalization standards and data augmentation methods established in Model 1.
   - The hyperparameter configuration mirrored that of Model 1.

Both models' outputs, encompassing classification and segmentation, were binary thresholded to yield discrete values of 0 or 1 (threshold=0.5). The datasets were divided into three cohorts for model training, validation, and testing, with a distribution of 60%, 20%, and 20%, respectively.

The models' performance was evaluated using an array of metrics:

- For classification: Average precision, ROC AUC, balanced accuracy, specificity, and sensitivity.
- For segmentation: Intersection over Union (IOU).

The computational framework was reliant on the following dependencies: TensorFlow version 2.14.0, Keras-UNET Collection, Pandas, Sacred, Albumentations, Pynrrd, and Scikit-learn.

Statistical analysis

Categorical variables were represented as absolute numbers and percentages, while continuous variables were reported using the median and interquartile range in instances of skewed distributions, or as mean values with standard deviation (± SD) in cases of normal distribution.

The distribution of continuous variables was determined using the Kolmogorov-Smirnov test. For comparisons between two groups, continuous variables were assessed using the Student's t-test or the Mann-Whitney U test, depending on the nature of the continuous data. The association between continuous variables was quantified using Spearman's correlation coefficient. Qualitative data were compared using the Chi-square ($\chi 2$) test or Fisher's exact test, contingent upon the expected cell counts.

A Receiver Operating Characteristic (ROC) curve analysis was employed to evaluate arterial phase enhancement in contrast-enhanced computed tomography (CE-CT) as a predictor of microvessel density (MVD) and to ascertain the optimal cutoff point for preoperative identification of patients with high or low MVD. The overall efficacy was presented as the area under the curve with a 95% confidence interval. Both univariate and multivariate logistic regression analyses were performed to identify preoperative predictors of low MVD.

Disease-Free Survival (DFS) was defined as the period from surgery to the first indication of disease recurrence as identified by imaging. Overall Survival (OS) was determined as the time from surgery to death from any cause, while Disease-Specific Survival (DSS) referred to the time from surgery to death attributed to the disease. DFS, OS, and DSS were tracked until the last follow-up or until the occurrence of events. Survival probabilities were estimated using the Kaplan-Meier method, and differences in DFS between patients with high or low MVD were compared using the log-rank test.

All statistical analyses were conducted using MedCalc version 13 (MedCalc Software, Belgium).

REFERENCES

[Anatomia umana] / Giuseppe C. Balboni ...[et al.] - Università degli Studi di Firenze

Agarwal B, Abu-Hamda E, Molke KL, Correa AM & Ho L (2004) Endoscopic ultrasound-guided fine needle aspiration and multidetector spiral CT in the diagnosis of pancreatic cancer. *Am J Gastroenterol* 99: 844–850

Ainsworth AP, Rafaelsen SR, Wamberg PA, Durup J, Pless TK & Mortensen MB (2003) Is there a difference in diagnostic accuracy and clinical impact between endoscopic ultrasonography and magnetic resonance cholangiopancreatography? *Endoscopy* 35: 1029–1032

Archibugi L, Ruta V, Panzeri V, Redegalli M, Testoni SGG, Petrone MC, Rossi G, Falconi M, Reni M, Doglioni C, *et al* (2020) RNA Extraction from Endoscopic Ultrasound-Acquired Tissue of Pancreatic Cancer Is Feasible and Allows Investigation of Molecular Features. *Cells* 9

Bailey P, Chang DK, Nones K, Johns AL, Patch AM, Gingras MC, Miller DK, Christ AN, Bruxner TJC, Quinn MC, *et al* (2016) Genomic analyses identify molecular subtypes of pancreatic cancer. *Nature* 531: 47–52

Banafea O, Mghanga FP, Zhao J, Zhao R & Zhu L (2016) Endoscopic ultrasonography with fine-needle aspiration for histological diagnosis of solid pancreatic masses: A meta-analysis of diagnostic accuracy studies. *BMC Gastroenterol* 16

Barresi L, Tacelli M, Tarantino I, Cipolletta F, Granata A & Traina M (2018) Improving the yield of EUS-guided histology. *Endosc Ultrasound* 7: 301–305

Berry W, Algar E, Kumar B, Desmond C, Swan M, Jenkins BJ & Croagh D (2017) Endoscopic ultrasound-guided fine-needle aspirate-derived preclinical pancreatic cancer models reveal panitumumab sensitivity in KRAS wild-type tumors. *Int J Cancer* 140: 2331–2343

Bilimoria KY, Bentrem DJ, Merkow RP, Tomlinson JS, Stewart AK, Ko CY & Talamonti MS (2007) Application of the pancreatic adenocarcinoma staging system to pancreatic neuroendocrine tumors. *J Am Coll Surg* 205: 558–563

Borbath I, Van Beers BE, Lonneux M, Schoonbroodt D, Geubel A, Gigot JF & Deprez PH (2005) Preoperative assessment of pancreatic tumors using magnetic resonance imaging, endoscopic ultrasonography, positron emission tomography and laparoscopy. *Pancreatology* 5: 553–561

Canto MI, Goggins M, Yeo CJ, Griffin C, Axilbund JE, Brune K, Ali SZ, Jagannath S, Petersen GM, Fishman EK, *et al* (2004) Screening for pancreatic neoplasia in high-risk individuals: An EUS-based approach. *Clinical Gastroenterology and Hepatology* 2: 606–621

Canto MI, Hruban RH, Fishman EK, Kamel IR, Schulick R, Zhang Z, Topazian M, Takahashi N, Fletcher J, Petersen G, *et al* (2012) Frequent detection of pancreatic lesions in asymptomatic high-risk individuals. *Gastroenterology* 142: 796–804

Cappelli C, Boggi U, Mazzeo S, Cervelli R, Campani D, Funel N, Contillo BP & Bartolozzi C (2015) Contrast enhancement pattern on multidetector CT predicts malignancy in pancreatic endocrine tumours. *Eur Radiol* 25: 751–759

Carrara S, Soldà G, Di Leo M, Rahal D, Peano C, Giunta M, Lamonaca L, Auriemma F, Anderloni A, Fugazza A, *et al* (2021) Side-by-side comparison of next-generation sequencing, cytology, and histology in diagnosing locally advanced pancreatic adenocarcinoma. *Gastrointest Endosc* 93: 597-604.e5

Casolino R, Braconi C, Malleo G, Paiella S, Bassi C, Milella M, Dreyer SB, Froeling FEM, Chang DK, Biankin A V., *et al* (2021) Reshaping preoperative treatment of pancreatic cancer in the era of precision medicine. *Ann Oncol* 32: 183–196

Chen J, Yang R, Lu Y, Xia Y & Zhou H (2012) Diagnostic accuracy of endoscopic ultrasound-guided fine-needle aspiration for solid pancreatic lesion: A systematic review. *J Cancer Res Clin Oncol* 138: 1433–1441 doi:10.1007/s00432-012-1268-1 [PREPRINT]

Cives M & Strosberg JR (2018) Gastroenteropancreatic Neuroendocrine Tumors. *CA Cancer J Clin* 68: 471–487

Collisson EA, Sadanandam A, Olson P, Gibb WJ, Truitt M, Gu S, Cooc J, Weinkle J, Kim GE, Jakkula L, *et al* (2011) Subtypes of pancreatic ductal adenocarcinoma and their differing responses to therapy. *Nat Med* 17: 500–503

Couvelard A, Deschamps L, Ravaud P, Baron G, Sauvanet A, Hentic O, Colnot N, Paradis V, Belghiti J, Bedossa P, *et al* (2009) Heterogeneity of tumor prognostic markers: a reproducibility study applied to liver metastases of pancreatic endocrine tumors. *Mod Pathol* 22: 273–281

Couvelard A, Deschamps L, Rebours V, Sauvanet A, Gatter K, Pezzella F, Ruszniewski P & Bedossa P (2008) Overexpression of the oxygen sensors PHD-1, PHD-2, PHD-

3, and FIH Is associated with tumor aggressiveness in pancreatic endocrine tumors. *Clin Cancer Res* 14: 6634–6639

Dahiya DS, Al-Haddad M, Chandan S, Gangwani MK, Aziz M, Mohan BP, Ramai D, Canakis A, Bapaye J & Sharma N (2022) Artificial Intelligence in Endoscopic Ultrasound for Pancreatic Cancer: Where Are We Now and What Does the Future Entail? *J Clin Med* 11

Das A, Nguyen CC, Li F & Li B (2008) Digital image analysis of EUS images accurately differentiates pancreatic cancer from chronic pancreatitis and normal tissue. *Gastrointest Endosc* 67: 861–867

Dasari A, Shen C, Halperin D, Zhao B, Zhou S, Xu Y, Shih T & Yao JC (2017) Trends in the Incidence, Prevalence, and Survival Outcomes in Patients With Neuroendocrine Tumors in the United States. *JAMA Oncol* 3: 1335–1342

D'Assignies G, Couvelard A, Bahrami S, Vullierme MP, Hammel P, Hentic O, Sauvanet A, Bedossa P, Ruszniewski P & Vilgrain V (2009) Pancreatic endocrine tumors: tumor blood flow assessed with perfusion CT reflects angiogenesis and correlates with prognostic factors. *Radiology* 250: 407–416

DeWitt J, Devereaux B, Chriswell M, McGreevy K, Howard T, Imperiale TF, Ciaccia D, Lane KA, Maglinte D, Kopecky K, *et al* (2004) Comparison of endoscopic ultrasonography and multidetector computed tomography for detecting and staging pancreatic cancer. *Ann Intern Med* 141

Dietrich CF, Ignee A & Frey H (2005) Contrast-enhanced endoscopic ultrasound with low mechanical index: A new technique. *Z Gastroenterol* 43: 1219–1223

Dimagno EP, Regan PT, Wilson DA, Buxton JL, Hattery RR, Suarez JR & Green PS (1980) Ultrasonic endoscope. *Lancet* 1: 629–631

Ducreux M, Cuhna AS, Caramella C, Hollebecque A, Burtin P, Goéré D, Seufferlein T, Haustermans K, Van Laethem JL, Conroy T, *et al* (2015) Cancer of the pancreas: ESMO Clinical Practice Guidelines for diagnosis, treatment and follow-up. *Annals of Oncology* 26: v56–v68

Dumonceau JM, Deprez PH, Jenssen C, Iglesias-Garcia J, Larghi A, Vanbiervliet G, Aithal GP, Arcidiacono PG, Bastos P, Carrara S, *et al* (2017) Indications, results, and clinical impact of endoscopic ultrasound (EUS)-guided sampling in gastroenterology: European Society of Gastrointestinal Endoscopy (ESGE) Clinical

Guideline - Updated January 2017. *Endoscopy* 49: 695–714 doi:10.1055/s-0043-109021 [PREPRINT]

Falconi M, Eriksson B, Kaltsas G, Bartsch DK, Capdevila J, Caplin M, Kos-Kudla B, Kwekkeboom D, Rindi G, KlÖppel G, *et al* (2016) ENETS consensus guidelines update for the management of patients with functional pancreatic neuroendocrine tumors and non-functional pancreatic neuroendocrine tumors. In *Neuroendocrinology* pp 153–171. S. Karger AG

Fujino M, Aishima S, Shindo K, Oda Y, Morimatsu K, Tsutsumi K, Otsuka T, Tanaka M & Oda Y (2016) Expression of glucose transporter-1 is correlated with hypoxia-inducible factor 1α and malignant potential in pancreatic neuroendocrine tumors. *Oncol Lett* 12: 3337–3343

Gleeson FC, Levy MJ, Jackson RA, Murphy SJ, Halling KC, Kipp BR, Graham RP & Zhang L (2020) Endoscopic ultrasound may be used to deliver gene expression signatures using digital mRNA detection methods to immunophenotype pancreatic ductal adenocarcinoma to facilitate personalized immunotherapy. *Pancreatology* 20: 229–238

Goh BKP, Chow PKH, Tan YM, Cheow PC, Chung YFA, Soo KC, Wong WK & Ooi LLPJ (2011) Validation of five contemporary prognostication systems for primary pancreatic endocrine neoplasms: results from a single institution experience with 61 surgically treated cases. *ANZ J Surg* 81: 79–85

Gong TT, Hu DM & Zhu Q (2012) Contrast-enhanced EUS for differential diagnosis of pancreatic mass lesions: A meta-analysis. *Gastrointest Endosc* 76: 301–309

Goyal H, Sherazi SAA, Gupta S, Perisetti A, Achebe I, Ali A, Tharian B, Thosani N & Sharma NR (2022) Application of artificial intelligence in diagnosis of pancreatic malignancies by endoscopic ultrasound: a systemic review. *Therap Adv Gastroenterol* 15

Habib JR, Zhu Y, Yin L, Javed AA, Ding D, Tenior J, Wright M, Ali SZ, Burkhart RA, Burns W, *et al* (2021) Reliable Detection of Somatic Mutations for Pancreatic Cancer in Endoscopic Ultrasonography-Guided Fine Needle Aspirates with Next-Generation Sequencing: Implications from a Prospective Cohort Study. *J Gastrointest Surg* 25: 3149–3159

Hallet J, Law CHL, Cukier M, Saskin R, Liu N & Singh S (2015) Exploring the rising incidence of neuroendocrine tumors: a population-based analysis of epidemiology, metastatic presentation, and outcomes. *Cancer* 121: 589–597

Harewood GC & Wiersema MJ (2002) Endosonography-guided fine needle aspiration biopsy in the evaluation of pancreatic masses. *Am J Gastroenterol* 97: 1386–1391

Harinck F, Konings ICAW, Kluijt I, Poley JW, Van Hooft JE, Van Dullemen HM, Nio CY, Krak NC, Hermans JJ, Aalfs CM, *et al* (2016) A multicentre comparative prospective blinded analysis of EUS and MRI for screening of pancreatic cancer in high-risk individuals. *Gut* 65: 1505–1513

He XK, Ding Y & Sun LM (2017) Contrast-enhanced endoscopic ultrasound for differential diagnosis of pancreatic cancer: An updated meta-analysis. *Oncotarget* 8: 66392–66401

Hewitt MJ, McPhail MJW, Possamai L, Dhar A, Vlavianos P & Monahan KJ (2012) EUS-guided FNA for diagnosis of solid pancreatic neoplasms: A meta-analysis. *Gastrointest Endosc* 75: 319–331

Iglesias-Garcia J, Lariño-Noia J, Abdulkader I & Domínguez-Muñoz JE (2014) Rapid on-site evaluation of endoscopic-ultrasound-guided fine-needle aspiration diagnosis of pancreatic masses. *World J Gastroenterol* 20: 9451–9457

Jensen RT, Berna MJ, Bingham DB & Norton JA (2008) Inherited pancreatic endocrine tumor syndromes: advances in molecular pathogenesis, diagnosis, management, and controversies. *Cancer* 113: 1807–1843

Kamata K, Kitano M, Kudo M, Sakamoto H, Kadosaka K, Miyata T, Imai H, Maekawa K, Chikugo T, Kumano M, *et al* (2014) Value of EUS in early detection of pancreatic ductal adenocarcinomas in patients with intraductal papillary mucinous neoplasms. *Endoscopy* 46: 22–29

Kim C, Byun JH, Hong SM, An S, Kim JH, Lee SS & Kim HJ (2017) A comparison of enhancement patterns on dynamic enhanced CT and survival between patients with pancreatic neuroendocrine tumors with and without intratumoral fibrosis. *Abdom Radiol (NY)* 42: 2835–2842

Kimura W, Kuroda A & Morioka Y (1991) Clinical pathology of endocrine tumors of the pancreas. Analysis of autopsy cases. *Dig Dis Sci* 36: 933–942

Kitano M, Yoshida T, Itonaga M, Tamura T, Hatamaru K & Yamashita Y (2019) Impact of endoscopic ultrasonography on diagnosis of pancreatic cancer. *J Gastroenterol* 54: 19–32

Klimstra DS, Modlin IR, Coppola D, Lloyd R V. & Suster S (2010) The Pathologic Classification of Neuroendocrine Tumors. *Pancreas* 39: 707–712

Klöppel G, Klimstra DS, Hruban RH, Adsay V, Capella C, Couvelard A, Komminoth P, Rosa S La, Ohike N, Osamura RY, *et al* (2017) Pancreatic Neuroendocrine Tumors: Update on the New World Health Organization Classification. *AJSP Rev Rep* 22: 233–239

Koul A, Baxi AC, Shang R, Meng X, Li L, Keilin SA, Willingham FF & Cai Q (2018) The efficacy of rapid on-site evaluation during endoscopic ultrasound-guided fine needle aspiration of pancreatic masses. *Gastroenterol Rep (Oxf)* 6: 45–48

Krishna SG, Rao BB, Ugbarugba E, Shah ZK, Blaszczak A, Hinton A, Conwell DL & Hart PA (2017) Diagnostic performance of endoscopic ultrasound for detection of pancreatic malignancy following an indeterminate multidetector CT scan: a systemic review and meta-analysis. *Surg Endosc* 31: 4558–4567

Kuwahara T, Hara K, Mizuno N, Okuno N, Matsumoto S, Obata M, Kurita Y, Koda H, Toriyama K, Onishi S, *et al* (2019) Usefulness of Deep Learning Analysis for the Diagnosis of Malignancy in Intraductal Papillary Mucinous Neoplasms of the Pancreas. *Clin Transl Gastroenterol* 10

Larghi A, Lawlor RT, Crinò SF, Luchini C, Rizzatti G, Curatolo M, Gabbrielli A, Inzani F & Scarpa A (2020) Endoscopic ultrasound guided fine needle biopsy samples to drive personalized medicine: A proof of concept study. *Pancreatology* 20: 778–780

Lawrence B, Gustafsson BI, Chan A, Svejda B, Kidd M & Modlin IM (2011) The Epidemiology of Gastroenteropancreatic Neuroendocrine Tumors. *Endocrinol Metab Clin North Am* 40: 1–18

Li X, Xu W, Shi J, Lin Y & Zeng X (2013) Endoscopic ultrasound elastography for differentiating between pancreatic adenocarcinoma and inflammatory masses: A meta-analysis. *World J Gastroenterol* 19: 6284–6291

Loos M, Michalski CW & Kleeff J (2012) Asymptomatic pancreatic lesions: new insights and clinical implications. *World J Gastroenterol* 18: 4474–7

Lundy J, Gao H, Berry W, Masoumi-Moghoddam S, Jenkins BJ & Croagh D (2021) Targeted Transcriptome and KRAS Mutation Analysis Improve the Diagnostic Performance of EUS-FNA Biopsies in Pancreatic Cancer. *Clin Cancer Res* 27: 5900–5911

Masugi Y (2022) The Desmoplastic Stroma of Pancreatic Cancer: Multilayered Levels of Heterogeneity, Clinical Significance, and Therapeutic Opportunities. *Cancers (Basel)* 14

Mei M, Ni J, Liu D, Jin P & Sun L (2013) EUS elastography for diagnosis of solid pancreatic masses: A meta-analysis. *Gastrointest Endosc* 77: 578–589

Metz DC & Jensen RT (2008) Gastrointestinal neuroendocrine tumors: pancreatic endocrine tumors. *Gastroenterology* 135: 1469–92

Moffitt RA, Marayati R, Flate EL, Volmar KE, Loeza SGH, Hoadley KA, Rashid NU, Williams LA, Eaton SC, Chung AH, *et al* (2015) Virtual microdissection identifies distinct tumor- and stroma-specific subtypes of pancreatic ductal adenocarcinoma. *Nat Genet* 47: 1168–1178

Müller MF, Meyenberger C, Bertschinger P, Schaer R & Marincek B (1994) Pancreatic tumors: evaluation with endoscopic US, CT, and MR imaging. *Radiology* 190: 745–751

Napoleon B, Alvarez-Sanchez M V., Gincoul R, Pujol B, Lefort C, Lepilliez V, Labadie M, Souquet JC, Queneau PE, Scoazec JY, *et al* (2010) Contrast-enhanced harmonic endoscopic ultrasound in solid lesions of the pancreas: Results of a pilot study. *Endoscopy* 42: 564–570

Navina S, McGrath K, Chennat J, Singh V, Pal T, Zeh H & Krasinskas AM (2014) Adequacy assessment of endoscopic ultrasound-guided, fine-needle aspirations of pancreatic masses for theranostic studies: Optimization of current practices is warranted. *Arch Pathol Lab Med* 138: 923–928

Nawaz H, Yi-Fan C, Kloke J, Khalid A, McGrath K, Landsittel D & Papachristou GI (2013) Performance characteristics of endoscopic ultrasound in the staging of pancreatic cancer: A meta-analysis. *Journal of the Pancreas* 14: 484–497

Neesse A, Bauer CA, Öhlund D, Lauth M, Buchholz M, Michl P, Tuveson DA & Gress TM (2019) Stromal biology and therapy in pancreatic cancer: ready for clinical translation? *Gut* 68: 159–171

Ntellas P, Dadouli K, Perivoliotis K, Sogka E, Pentheroudakis G, Ioannou M, Hadjichristodoulou C, Tepetes K & Mauri D (2019) Microvessel Density and Impact of Angiogenesis on Survival of Resected Pancreatic Cancer Patients: A Systematic Review and Meta-analysis. *Pancreas* 48: 233–241

Okusaka T, Nakamura M, Yoshida M, Kitano M, Uesaka K, Ito Y, Furuse J, Hanada K & Okazaki K (2020) Clinical Practice Guidelines for Pancreatic Cancer 2019 from the Japan Pancreas Society: A Synopsis. *Pancreas* 49: 326–335 doi:10.1097/MPA.0000000000001513 [PREPRINT]

Palazzo M, Napoléon B, Gincul R, Pioche M, Pujol B, Lefort C, Fumex F, Hautefeuille V, Fabre M, Cros J, *et al* (2018) Contrast harmonic EUS for the prediction of pancreatic neuroendocrine tumor aggressiveness (with videos). *Gastrointest Endosc* 87: 1481–1488

De Palma M, Biziato D & Petrova T V. (2017) Microenvironmental regulation of tumour angiogenesis. *Nat Rev Cancer* 17: 457–474

Panch T, Szolovits P & Atun R (2018) Artificial intelligence, machine learning and health systems. *J Glob Health* 8

Partelli S, Giannone F, Schiavo Lena M, Muffatti F, Andreasi V, Crippa S, Tamburrino D, Zamboni G, Rubini C, Doglioni C, *et al* (2019) Is the Real Prevalence of Pancreatic Neuroendocrine Tumors Underestimated? A Retrospective Study on a Large Series of Pancreatic Specimens. *Neuroendocrinology* 109: 165–170

Pei Q, Zou X, Zhang X, Chen M, Guo Y & Luo H (2012) Diagnostic value of EUS elastography in differentiation of benign and malignant solid pancreatic masses: A meta-analysis. *Pancreatology* 12: 402–408

Perri G, Prakash LR & Katz MHG (2019) Pancreatic neuroendocrine tumors. *Curr Opin Gastroenterol* 35: 468–477

Poncet G, Villaume K, Walter T, Pourreyron C, Theillaumas A, Lépinasse F, Hervieu V, Cordier-Bussat M, Scoazec JY & Roche C (2009) Angiogenesis and tumor progression in neuroendocrine digestive tumors. *J Surg Res* 154: 68–77

Puleo F, Nicolle R, Blum Y, Cros J, Marisa L, Demetter P, Quertinmont E, Svrcek M, Elarouci N, Iovanna J, *et al* (2018) Stratification of Pancreatic Ductal Adenocarcinomas Based on Tumor and Microenvironment Features. *Gastroenterology* 155: 1999-2013.e3

Puli SR, Kalva N, Bechtold ML, Pamulaparthy SR, Cashman MD, Estes NC, Pearl RH, Volmar FH, Dillon S, Shekleton MF, *et al* (2013) Diagnostic accuracy of endoscopic ultrasound in pancreatic neuroendocrine tumors: A systematic review and meta analysis. *World J Gastroenterol* 19: 3678–3684

Rasmussen LG, Verbeke CS, Sørensen MD, Pfeiffer P, Tan Q, Mortensen MB, Fristrup C & Detlefsen S (2021) Gene expression profiling of morphologic subtypes of pancreatic ductal adenocarcinoma using surgical and EUS-FNB specimens. *Pancreatology* 21: 530–543

Rindi G, Falconi M, Klersy C, Albarello L, Boninsegna L, Buchler MW, Capella C, Caplin M, Couvelard A, Doglioni C, *et al* (2012a) TNM Staging of Neoplasms of the Endocrine Pancreas: Results From a Large International Cohort Study. *JNCI: Journal of the National Cancer Institute* 104: 764–777

Rindi G, Falconi M, Klersy C, Albarello L, Boninsegna L, Buchler MW, Capella C, Caplin M, Couvelard A, Doglioni C, *et al* (2012b) TNM staging of neoplasms of the endocrine pancreas: results from a large international cohort study. *J Natl Cancer Inst* 104: 764–777

Săftoiu A, Vilmann P, Gorunescu F, Janssen J, Hocke M, Larsen M, Iglesias-Garcia J, Arcidiacono P, Will U, Giovannini M, *et al* (2012) Efficacy of an artificial neural network-based approach to endoscopic ultrasound elastography in diagnosis of focal pancreatic masses. *Clin Gastroenterol Hepatol* 10

Schmidt RL, Walker BS, Howard K, Layfield LJ & Adler DG (2013) Rapid on-site evaluation reduces needle passes in endoscopic ultrasound-guided fine-needle aspiration for solid pancreatic lesions: A risk-benefit analysis. *Dig Dis Sci* 58: 3280–3286

Schmitt AM, Schmid S, Rudolph T, Anlauf M, Prinz C, Klöppel G, Moch H, Heitz PU, Komminoth P & Perren A (2009) VHL inactivation is an important pathway for the development of malignant sporadic pancreatic endocrine tumors. *Endocr Relat Cancer* 16: 1219–1227

Scoazec JY (2013) Angiogenesis in neuroendocrine tumors: therapeutic applications. *Neuroendocrinology* 97: 45–56

Səftoiu A, Vilmann P, Dietrich CF, Iglesias-Garcia J, Hocke M, Seicean A, Ignee A, Hassan H, Streba CT, Ioncicə AM, *et al* (2015) Quantitative contrast-enhanced

harmonic EUS in differential diagnosis of focal pancreatic masses (with videos). *Gastrointest Endosc* 82: 59–69

Siddiqui AA, Brown LJ, Hong SKS, Draganova-Tacheva RA, Korenblit J, Loren DE, Kowalski TE & Solomides C (2011) Relationship of pancreatic mass size and diagnostic yield of endoscopic ultrasound-guided fine needle aspiration. *Dig Dis Sci* 56: 3370–3375

Sorbye H, Strosberg J, Baudin E, Klimstra DS & Yao JC (2014) Gastroenteropancreatic high-grade neuroendocrine carcinoma. *Cancer* 120: 2814–2823

Tacelli M, Bina N, Crinò SF, Facciorusso A, Celsa C, Vanni AS, Fantin A, Antonini F, Falconi M, Monica F, *et al* (2022) Reliability of grading preoperative pancreatic neuroendocrine tumors on EUS specimens: a systematic review with meta-analysis of aggregate and individual data. *Gastrointest Endosc* 96: 898-908.e23

Tacelli M, Petrone M, Capurso G, Muffatti F, Andreasi V, Partelli S, Doglioni C, Falconi M & Arcidiacono P (2021) Diagnostic accuracy of EUS-FNA in the evaluation of pancreatic neuroendocrine neoplasms grading: Possible clinical impact of misclassification. *Endosc Ultrasound* 10: 372–380

Uehara H, Ikezawa K, Kawada N, Fukutake N, Katayama K, Takakura R, Takano Y, Ishikawa O & Takenaka A (2011) Diagnostic accuracy of endoscopic ultrasound-guided fine needle aspiration for suspected pancreatic malignancy in relation to the size of lesions. *Journal of Gastroenterology and Hepatology (Australia)* 26: 1256–1261

Xu W, Shi J, Li X, Zeng X & Lin Y (2013) Endoscopic ultrasound elastography for differentiation of benign and malignant pancreatic masses: A systemic review and meta-analysis. *Eur J Gastroenterol Hepatol* 25: 218–224

Yamada R, Tsuboi J, Murashima Y, Tanaka T, Nose K & Nakagawa H (2023) Advances in the Early Diagnosis of Pancreatic Ductal Adenocarcinoma and Premalignant Pancreatic Lesions. *Biomedicines* 11

Yao JC, Hassan M, Phan A, Dagohoy C, Leary C, Mares JE, Abdalla EK, Fleming JB, Vauthey JN, Rashid A, *et al* (2008) One hundred years after ‘carcinoid’: epidemiology of and prognostic factors for neuroendocrine tumors in 35,825 cases in the United States. *J Clin Oncol* 26: 3063–3072

Ying L, Lin X, Xie ZL, Hu YP, Tang KF & Shi KQ (2013) Clinical utility of endoscopic ultrasound elastography for identification of malignant pancreatic masses: A meta-analysis. *Journal of Gastroenterology and Hepatology (Australia)* 28: 1434–1443 doi:10.1111/jgh.12292 [PREPRINT]

Zheng-Lin B & O'Reilly EM (2021) Pancreatic ductal adenocarcinoma in the era of precision medicine. *Semin Oncol* 48: 19–33